ELSEVIER

Chemical Geology 198 (2003) 107–137

CHEMICAL GEOLOGY
INCLUDING
ISOTOPE GEOSCIENCE

www.elsevier.com/locate/chemgeo

# Compositional and structural control of fission-track annealing in apatite

Jocelyn Barbarand[1], Andrew Carter, Ian Wood, Tony Hurford*

*Research School of Earth Sciences at University College London and Birkbeck College, Gower Street, London WC1E 6BT, UK*

Received 18 April 2002; accepted 6 December 2002

**Abstract**

Geological cooling histories modelled from apatite fission-track (FT) data are dependent upon extrapolated, laboratory-based track annealing data. Annealing in apatite appears to be compositionally controlled. This study investigates how compositional variation influences apatite crystal structure (as reflected in the unit-cell parameters) and fission-track annealing, and then considers how best to monitor bulk composition in a practical way for routine fission-track analysis.

New fission-track annealing data are presented for a series of 10-, 100- and 1000-h experiments on 13 apatite samples of different chemical composition. The bulk apatite composition of these samples was determined using uranium mapping, cathodoluminescence (CL), electron microprobe, inductively coupled plasma mass spectrometry (ICP-MS), inductively coupled plasma atomic emission spectrometry (ICP-AES) and spectrophotometry techniques, and their cell parameters characterised by X-ray powder diffractometry (XRD).

Apatite structure reflects apatite bulk composition and unit-cell dimensions are changed by the complex interactions between anion substitutions (Cl, F, OH) and cation substitution (REE, Mn, Sr). While chlorine has a dominant control on apatite structure above 0.1 anion per formula unit ($\sim$ 0.35 wt.%), below this value other elements, in particular REE, exert a significant control. This study shows that the rate of fission-track annealing correlates with apatite structure, the annealing rate being slower for crystals with larger values for cell parameter *a* and smaller values for cell parameter *c*. In an earlier study, Carlson et al. [Am. Mineral. 84 (1999) 1213] found this correlation to be valid only for apatites of certain compositions.

Ideally, the bulk composition and/or unit cell should be measured for each apatite grain analysed by the fission-track method to determine the appropriate track annealing parameters for use in thermal history prediction. Neither approach is a practical reality for routine analysis. The relative merits of determining chlorine content, the major influence on fission-track annealing, and using apatite solubility by measuring etch-pit sizes are discussed as practical alternatives for assessing the annealing response of individual apatite crystals.


*Keywords:* Apatite fission-track thermochronology; Fission-track annealing; Apatite composition; Unit-cell parameters; Thermal history prediction

## 1. Introduction

Apatite fission-track (FT) analysis is a widely used thermochronometric technique that enables geologists to reconstruct low-temperature thermal histories of

* Corresponding author. Tel.: +44-20-7679-7704; fax: +44-20-7813-2802.

*E-mail address:* t.hurford@ucl.ac.uk (T. Hurford).

[1] Present address: Département des Sciences de la Terre, Batiment 504, Université Paris Sud, F-91405 Orsay-Cedex, France.

0009-2541/03/$ - see front matter © 2003 Elsevier Science B.V. All rights reserved.
doi:10.1016/S0009-2541(02)00424-2

upper crustal rocks. It is extensively used in tectonic geomorphology to study orogenic belt and rift zone evolution, in sedimentology to monitor timing and volume of sediment supply and in hydrocarbon exploration to assess hydrocarbon maturity (see review in Gallagher et al., 1998). Extraction of thermochronological information is based on using measured FT age and length data with a modelling program to predict thermal histories most consistent with the measured sample data. The modelling procedure uses annealing models that aim to describe the quantitative relationship between the FT age and track-length parameters, and temperature and time. The first published apatite annealing model using confined track-length measurement (Laslett et al., 1987) was based on laboratory experiments using the Durango apatite, where Cl = 0.12 anion per formula unit (apfu) equivalent to 0.41 wt.%, and a fluorine content broadly similar to apatites found in most common rock types. Model extrapolations to geological timescales were verified against geological observations, based on drill hole samples from the Mesozoic Otway Basin in southeastern Australia (Green et al., 1989).

At about the same time as the first annealing experiments using FT length were taking place, geological observation indicated that apatite composition could have a major control on fission-track annealing rate. Gleadow and Duddy (1981) recorded significant dispersion between apatite grain ages in samples from drill-holes in the Otway basin, which was attributed to different apatite compositions. Subsequently, Green et al. (1985, 1986) demonstrated that apparent apatite FT ages in Otway Basin sediments could be correlated with chlorine content and it was observed that, for the same thermal history, Cl-rich apatite grains showed less FT annealing than F-rich apatites.

The importance of apatite composition has been the focus of more recent attempts to improve FT annealing models based on the knowledge that numerous elements may be substituted into the Ca, P or anion sites of apatite $Ca_{10}(PO_4)_6(F,Cl,OH)$ (Elliott, 1994). These studies, using laboratory and geological observation, have confirmed the dominant control of chlorine on FT annealing (e.g. Crowley et al., 1990; O'Sullivan and Parrish, 1995), but also have established that other elements may cause differences in annealing. These substitutions include: Mn, Sr and Fe (Ravenhurst et al., 1993; Burtner et al., 1994; Carlson et al., 1999), rare earth elements (Carpéna, 1998; Barbarand and Pagel, 2001a), OH (Bergman and Corrigan, 1996), $CO_3$ (Ben Ghouma, 1995) and $SiO_2$ (Carpéna, 1998). The most detailed and comprehensive published annealing study to date (Carlson et al., 1999) concluded that annealing rates may be slower in samples with appreciable substitution of Ca by other cations. More importantly, it was noted that fission-track annealing rates are not singularly related to substitution of Ca by other cations, but, instead, may depend in a more complex manner on the level of mixing on the halogen site. This would imply that, to interpret apatite fission-track data fully, we need to determine the bulk composition of every single apatite grain upon which a FT age is measured, analytically a demanding task. The variable and multiple substitutions in apatite are reflected in differences in crystal structure and should be seen in variation of the unit-cell parameters. Thus, since FT annealing in apatite is compositionally dependent, it must also be structurally dependent.

In this paper, following the work of Carlson et al. (1999), we investigate further the relationships between apatite composition, crystal symmetry and unit-cell parameters, and fission-track annealing. In particular, we examine the case for determination of bulk composition and study the practicality of assessing apatite composition for routine FT sample analysis.

## 2. Substitution in apatite

Apatite composition is complex and variable. The formula for apatite can be expressed as $X_{10}YO_4Z_2$ where:

$$X = \text{mostly Ca},\ Y = P \text{ and } Z = F, Cl \text{ or } OH.$$

Widespread substitutions can occur on these three sites including most commonly $Fe^{2+}$, $Mn^{2+}$, $Na^{+}$, $REE^{3+}$, $Sr^{2+}$, $U^{4+}$ substituted on the X site, with Si, C and S substituted on the Y site. The substitution of trivalent cations (REE are generally present in large amounts in apatite, up to 1–2%) involves a coupled substitution to achieve charge balance and neutrality, e.g. (Rønsbo, 1989):

$$REE^{3+} + Si^{4+} \rightarrow Ca^{2+} + P^{5+} \text{ and}$$

$$REE^{3+} + Na^{+} \rightarrow 2Ca^{2+}.$$

Substitution for P by $CO_3^{2-}$ and $SO_4^{2-}$ is probably achieved by charge balancing on the Y site as (Binder and Troll, 1989):

$$3PO_4^{3-} \rightarrow SiO_4^{4-} + (SO_4^{2-}, CO_3^{2-}) + CO_3OH^{3-}.$$

Carbonate substitution is mostly found in sedimentary and carbonatite apatite (Liu and Comodi, 1993). Substitution of $O^{2-}$ on the Z site has also been proposed (Young and Munson, 1966). Each substitution is possible among apatite samples and may be characterised by different, possibly diagnostic REE/Si or Si/P ratios (Sommerauer and Katz-Lehnert, 1985; Rønsbo, 1989; Hughes et al., 1991a; Liu and Comodi, 1993; Seifert et al., 2000).

On the Z site, each atom is surrounded by three Ca atoms in one layer and, in addition, Ca–O columns are linked with $PO_4$ groups to form a hexagonal network. These two types of Ca sites [Ca(I) and Ca(II)] are characterised by different co-ordination polyhedra and bond lengths (Fig. 1). Elements substituted on the Ca site are split between these two sites as a function of their ionic radius and bonding energies (Fleet and Pan, 1995).

Most apatites have a hexagonal $P6_3/m$ structure. Within the unit cell, parameter $c$ corresponds to the elongation of the cell, parameter $a$ to the side of the base. Substitution on the Z site results in large variations in the cell dimensions with monoclinic variants for the Cl end-member (Hughes et al., 1989). Parameter $a$ varies from 9.367 Å for pure fluorapatite to 9.628 Å for chlorapatite; parameter $c$ varies in the opposite sense by roughly 50% of this amount, from 6.884 Å for pure fluorapatite to 6.764 Å for chlorapatite (Sudarsanan et al., 1972; Mackie et al., 1972). Other substitutions may be made on the Z site (Br, I, $NO_3^-$) and may therefore control change in apatite structure, but these elements are assumed to be very rare in apatite grown from geological melts (Elliott, 1994). Other substitutions such as $CO_3$, REE and $SiO_4$ have also been recognised as controlling the dimensions of the crystal lattice (LeGeros, 1965; Sommerauer and Katz-Lehnert, 1985; Liu and Comodi, 1993).

## 3. Apatite composition and structure: experiment and results

Carlson et al. (1999) have alluded to the interrelationship of composition, structure and FT annealing in apatite in their comment that annealing is governed in a complex way by mixing of elements in different sites. Our study aims to examine further

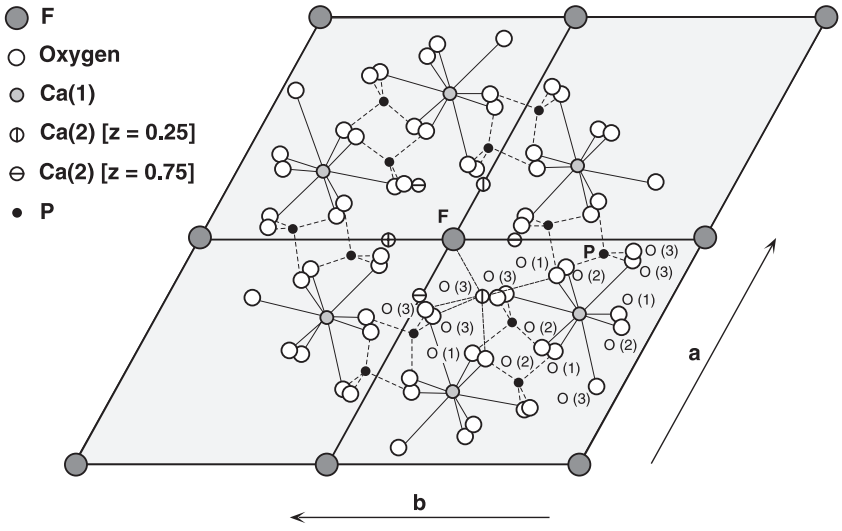


Fig. 1. Schematic representation of the crystal structure of apatite projected on the (001) plane. From Hughes et al. (1989).

how crystal structure responds to change in the bulk composition of apatite and then to consider how FT annealing relates to both apatite composition and structure. Accordingly, the bulk composition, unit-cell parameters and FT annealing parameters have been determined for a suite of apatites of varying composition.

### 3.1. Sample selection

From a collection of over 80 apatites, 13 samples were selected for study (Appendix A) with a spread of compositions considered representative of apatite from igneous, metamorphic and sedimentary sources (Bergman and Corrigan, 1996; Sha and Chappell, 1999), and which also complement apatite sample compositions used in previous studies (Green et al., 1986; Crowley et al., 1991; Carlson et al., 1999). In some cases, the same apatite was used as in previous studies to permit cross-calibration (e.g. DUR and FCT). Most samples were large single crystals, but two (FCT and GUN) were mineral separates.

Each sample was checked for compositional homogeneity both within and between grains. Uranium homogeneity was assessed by measuring the areal distribution of neutron-induced fission tracks (see below). Uranium concentration was also assessed for each sample by reference to Corning standard glass CN5 (U ~ 12 ppm) included in each irradiation. Cathodoluminescence (CL) spectroscopy was used to monitor the distribution of REE and Mn (Barbarand and Pagel, 2001b). Panchromatic CL images were obtained with an optical cathodoluminescence Technosyn Mark II microscope using 15–20 kV with an electron beam current between 200 and 400 mA. Sectors with different CL colours are diagnostic of elemental heterogeneity.

### 3.2. Sample composition

The diverse range of elements that may be present in apatite means that different analytical techniques are required to determine bulk composition since no single method can cover the full range of elements with adequate precision. Compositional data for the apatites studied are presented in Table 1. Major and minor elements were analysed by inductively coupled plasma atomic emission spectrometry (ICP-AES) with the exception of Cl, F and S, which were analysed by electron probe microanalysis (EPMA). Cl was also analysed by a spectrophotometric procedure for some low Cl concentration apatites as the detection limit of this method is lower than that of EPMA. Trace elements were determined by solution or laser inductively coupled plasma mass spectrometry (ICP-MS) depending on the amount of sample material available.

*ICP-AES* utilised a Jobin-Yvon JY 70 spectrometer to determine most major element compositions. Samples were fused with $LiBO_2$ and dissolved in $HNO_3$. Detection limits are $<0.2$ oxide wt.% for Si, $<0.1$ oxide wt.% for Al, Fe, Mg, Ca and $<0.05$ oxide wt.% for Mn, Na, K, Ti, P. Typical analytical precision was better than 1% of the measured values.

*EPMA* analyses were carried out using a wavelength-dispersive CAMECA SX50 employing the PAP matrix correction program. Operating conditions were 15 kV, with a beam current of 12 nA and a beam diameter of 5 μm. The two standard PET and TAP spectrometers were used to analyse, respectively, Cl to S and F to Si. Counting time was 30 s for F, 20 s for Cl, S and Si. Fluorine diffusion during the exposure of the beam was minimised by using a low beam current (12 nA), a short counting time and analysis of prismatic sections only (Stormer et al., 1993). Four to 10 replicate measurements were averaged for each grain analysed and no significant indication of crystal heterogeneity was found. Analyses, where the sum of the different oxides was lower than 98%, were rejected. Hydroxyl contents were determined by difference assuming a full occupancy of the halogen site by Cl, F and OH. Chemical formulae were calculated assuming 25 oxygen atoms. Detection limits for Cl, F, S and Si are, respectively, 0.03, 0.15, 0.05 and 0.02 oxide wt.% (Seifert et al., 2000).

*ICP-MS* was used to analyse the apatites for minor and trace element abundances. The majority of samples were analysed in solution using a Perkin Elmer 5000 ICP-MS. Typical precisions were better than 5% and detection limits were $<1$ ppm. Where only a limited amount of sample was available (FCT, GUN and LIN), analysis was undertaken using laser ablation ICP-MS. A Cetac LSX-100 frequency quadrupled (266 nm) Nd:YAG laser with an output power of 0.4 mJ was used. The laser beam was defocused 100 μm below the sample surface and the

Table 1
Composition, cell parameters and etch-pit measurements for the studied apatite samples

| | BAM | | DRV | | DUR | | FAR | | FCT | | FUL | | GIL | | GUN | | LIN | | MIN | | UMB | | UNK | | WIL | |
|---|---|---|---|---|---|---|---|---|---|---|---|---|---|---|---|---|---|---|---|---|---|---|---|---|---|---|
| | Oxide wt.% | Ion | Oxide wt.% | Ion | Oxide wt.% | Ion | Oxide wt.% | Ion | Oxide wt.% | Ion | Oxide wt.% | Ion | Oxide wt.% | Ion | Oxide wt.% | Ion | Oxide wt.% | Ion | Oxide wt.% | Ion | Oxide wt.% | Ion | Oxide wt.% | Ion | Oxide wt.% | Ion |
| *Chemical composition* | | | | | | | | | | | | | | | | | | | | | | | | | | |
| Ca | 53.02 | 9.80 | 54.14 | 10.01 | 54.69 | 9.90 | 56.13 | 10.00 | 54.53 | 9.80 | 55.23 | 9.96 | 55.73 | 10 | 54.64 | 9.89 | 51.83 | 9.53 | 55.04 | 9.95 | 55.32 | 9.93 | 54.88 | 9.93 | 54.48 | 9.76 |
| P | 40.99 | 5.99 | 38.52 | 5.63 | 41.19 | 5.89 | 42.22 | 5.94 | 41.50 | 5.89 | 41.70 | 5.94 | 41.55 | 5.91 | 41.51 | 5.93 | 42.05 | 6.11 | 39.81 | 5.69 | 42.30 | 6.00 | 41.33 | 5.91 | 41.83 | 5.92 |
| Cl | 4.67 | 1.37 | 0.01 | 0.00 | 0.39 | 0.11 | 0.01 | 0.00 | 0.83 | 0.24 | 0.71 | 0.20 | 0.031 | 0.01 | 1.54 | 0.44 | 2.01 | 0.58 | 0.02 | 0.01 | 0.41 | 0.12 | 0.002 | 0.00 | 0.00 | 0.00 |
| F | 0.06 | 0.03 | 3.21 | 1.75 | 3.53 | 1.89 | 3.58 | 1.88 | 1.72 | 0.91 | 1.87 | 0.99 | 1.02 | 0.54 | 1.75 | 0.93 | 1.60 | 0.87 | 2.16 | 1.15 | 1.48 | 0.78 | 2.76 | 1.47 | 3.40 | 1.80 |
| OH | 0.52 | 0.60 | 0.21 | 0.25 | 0.00 | 0.00 | 0.10 | 0.11 | 0.76 | 0.85 | 0.72 | 0.80 | 1.294 | 1.45 | 0.55 | 0.62 | 0.48 | 0.55 | 0.75 | 0.84 | 0.98 | 1.10 | 0.47 | 0.53 | 0.18 | 0.20 |
| Fe | 0.06 | 0.01 | 0.00 | 0.00 | 0.15 | 0.02 | 0.05 | 0.01 | 0.14 | 0.02 | 0.10 | 0.01 | 0.03 | 0.00 | 0.22 | 0.03 | 0.06 | 0.01 | 0.01 | 0.00 | 0.09 | 0.01 | 0.05 | 0.01 | 0.05 | 0.01 |
| Mn | 0.03 | 0.00 | 0.00 | 0.00 | 0.01 | 0.00 | 0.12 | 0.02 | 0.19 | 0.03 | 0.05 | 0.01 | 0.18 | 0.05 | 0.15 | 0.02 | 0.02 | 0.00 | 0.03 | 0.00 | 0.09 | 0.01 | 0.04 | 0.01 | 0.03 | 0.00 |
| Na | 0.32 | 0.11 | 0.09 | 0.03 | 0.31 | 0.10 | 0.17 | 0.05 | 0.12 | 0.04 | 0.07 | 0.02 | 0.04 | 0.01 | 0.10 | 0.03 | 0.17 | 0.06 | 0.10 | 0.03 | 0.05 | 0.02 | 0.21 | 0.07 | 0.32 | 0.10 |
| S | 0.07 | 0.01 | 0.62 | 0.08 | 0.21 | 0.03 | 0.00 | 0.00 | 0.42 | 0.05 | 0.12 | 0.02 | 0.03 | 0.01 | 0.00 | 0.00 | 0.00 | 0.00 | 1.22 | 0.15 | 0.00 | 0.00 | 0.27 | 0.03 | 0.35 | 0.04 |
| Si | 0.06 | 0.01 | 1.19 | 0.21 | 0.31 | 0.05 | 0.09 | 0.01 | 0.39 | 0.07 | 0.19 | 0.03 | 0.35 | 0.06 | 0.33 | 0.06 | 0.22 | 0.04 | 0.94 | 0.16 | 0.04 | 0.01 | 0.06 | 0.01 | 0.26 | 0.04 |
| Sr | 0.04 | 0.00 | 0.22 | 0.02 | 0.06 | 0.01 | 0.11 | 0.01 | 0.07 | 0.01 | 0.05 | 0.00 | 0.11 | 0.01 | 0.14 | 0.01 | 0.51 | 0.05 | 0.03 | 0.00 | 0.08 | 0.01 | 0.49 | 0.05 | 0.44 | 0.04 |
| Y | 0.34 | 0.03 | 0.13 | 0.01 | 0.06 | 0.01 | 0.00 | 0.00 | 0.00 | 0.00 | 0.02 | 0.00 | 0.01 | 0.00 | 0.00 | 0.00 | 0.00 | 0.00 | 0.03 | 0.00 | 0.03 | 0.00 | 0.05 | 0.00 | 0.05 | 0.00 |
| La | 0.12 | 0.01 | 0.38 | 0.02 | 0.44 | 0.03 | 0.07 | 0.00 | 0.30 | 0.02 | 0.17 | 0.01 | 0.01 | 0.00 | 0.20 | 0.01 | 0.07 | 0.00 | 0.05 | 0.00 | 0.00 | 0.00 | 0.17 | 0.01 | 0.23 | 0.01 |
| Ce | 0.34 | 0.02 | 0.95 | 0.06 | 0.53 | 0.03 | 0.26 | 0.02 | 0.56 | 0.03 | 0.21 | 0.01 | 0.01 | 0.00 | 0.44 | 0.03 | 0.21 | 0.01 | 0.11 | 0.01 | 0.00 | 0.00 | 0.38 | 0.02 | 0.51 | 0.03 |
| Pr | 0.04 | 0.00 | 0.12 | 0.01 | 0.04 | 0.00 | 0.03 | 0.00 | 0.05 | 0.00 | 0.02 | 0.00 | 0.01 | 0.00 | 0.05 | 0.00 | 0.02 | 0.00 | 0.01 | 0.00 | 0.00 | 0.00 | 0.04 | 0.00 | 0.06 | 0.00 |
| Nd | 0.17 | 0.01 | 0.44 | 0.03 | 0.13 | 0.01 | 0.10 | 0.01 | 0.16 | 0.01 | 0.05 | 0.00 | 0.01 | 0.00 | 0.19 | 0.01 | 0.08 | 0.00 | 0.05 | 0.00 | 0.01 | 0.00 | 0.16 | 0.01 | 0.21 | 0.01 |
| Sm | 0.04 | 0.00 | 0.06 | 0.00 | 0.02 | 0.00 | 0.02 | 0.00 | 0.02 | 0.00 | 0.01 | 0.00 | 0.01 | 0.00 | 0.03 | 0.00 | 0.01 | 0.00 | 0.01 | 0.00 | 0.00 | 0.00 | 0.02 | 0.00 | 0.03 | 0.00 |
| Σ | 100.34 | | 99.26 | | 100.64 | | 101.66 | | 101.61 | | 101.05 | | 101.5 | | 101.3 | | 98.70 | | 100.2 | | 101.2 | | 100.70 | | 101.18 | |
| Ca/P | | 1.66 | | 1.73 | | 1.69 | | 1.70 | | 1.66 | | 1.68 | | 1.70 | | 1.68 | | 1.57 | | 1.67 | | 1.66 | | 1.70 | | 1.66 |
| *Cell parameters, Å (± 1 S.E.M.)* | | | | | | | | | | | | | | | | | | | | | | | | | | |
| *a* | | | 9.3787 | (6) | 9.3896 | (6) | | | 9.4220** | (60) | 9.4047 | (10) | 9.4045 | (6) | 9.4615* | (20) | 9.4591 | (7) | 9.3963 | (7) | 9.4107 | (11) | 9.3709 | (4) | 9.370 | (4) |
| *c* | | | 6.8924 | (5) | 6.8790 | (5) | | | 6.8750 | (60) | 6.8739 | (6) | 6.8816 | (4) | 6.8491 | (20) | 6.8627 | (5) | 6.8898 | (5) | 6.8815 | (8) | 6.8879 | (3) | 6.887 | (3) |
| *Etch-pit size, μm (± 1 S.E.M.) ($D_{par}$)* | | | | | | | | | | | | | | | | | | | | | | | | | | |
| | 5.22 ± 0.04 | | 2.34 ± 0.03 | | 1.71 ± 0.03 | | 1.87 ± 0.03 | | 2.36 ± 0.03 | | 2.09 ± 0.02 | | 2.25 ± 0.04 | | 3.32 ± 0.03 | | 3.77 ± 0.03 | | 3.06 ± 0.03 | | 2.19 ± 0.03 | | 1.87 ± 0.02 | | 1.62 ± 0.03 | |

Chemical composition is expressed as oxide weight percent and number of atoms per formula unit (apfu). Total (Σ) is adjusted to account for F and Cl in place of O. Ca/P ratio corresponds to the ionic amount of Ca and atoms substituted for Ca, divided by the ionic amount of P and atoms substituted for P; the ratio represents a quality control of the data if apatite crystals are assumed to be stoichiometric (Ca/P = 1.66). The use of apfu to characterise the chemistry is therefore preferred. Etch-pit size parallel to the *c*-axis is in micrometer and each result is based on 100 measurements. *Cell parameter data for GUN from Hughes et al. (1990); **cell parameter data for FCT from Carlson et al. (1999).

shot repetition rate was set to 10 Hz. Data were collected over a 5-s interval for single spot analyses and over 30 s for rastered analyses. The ICP-MS used was the Surrey Research Instrument (NERC ICP-MS Facility, Kingston University) optimised under standard operating conditions and calibrating sample data against the NIST 610 glass with Ca as an internal standard.

A *wet chemistry spectrophotometric* procedure based on the absorption of orange-coloured ferric thiocyanate complex was also used to determine low levels of Cl in fluorapatite crystals. The basic chemical reactions involved are:

$$2Cl^- + Hg(SCN)_2 \rightarrow HgCl_2 + 2SCN^- \text{ and}$$

$$SCN^- + Fe^{3+} \rightarrow Fe(SCN)^{2+}$$

Analysis was carried out using a Beckman DU62 spectrophotometer using standard solutions. Detection limit is 20 ppm and analytical precision is ~ 5% for contents >100 ppm and ~ 20% for Cl concentration between 20 and 100 ppm. Agreement between these results and those of the electron microprobe is satisfactory for concentrations >0.1 apfu (~ 0.35 wt.%).

### 3.3. Sample structure: experiment and results

Powder X-ray diffractometry (XRD) was used to determine the unit-cell parameters of nine hexagonal apatite samples (Table 1). Three samples (FAR, FCT and GUN) for which insufficient sample was available have been excluded from XRD measurement in this study, although published XRD data for FCT and GUN (Carlson et al., 1999; Hughes et al., 1990) are included in Table 1 and are considered in the discussion. Data were collected in Bragg-Brentano reflection geometry using a computer-controlled Philips PW1050 goniometer and Fe-filtered Co Kα radiation at 35 kV and 35 mA. The data were collected in step-scanned mode covering the $2\theta$ range from 10° to 156° in steps of 0.025°; counting times were typically 13 s per point. Unit-cell dimensions were obtained by Rietveld refinement of the data using a version of the computer program LHPM1 (Hill and Howard, 1986) modified in-house to exclude explicitly the displacements of the diffraction peaks resulting from specimen displacement error, specimen transparency and axial and equatorial beam divergences of the diffractometer. These corrections are essential if cell parameters, which are accurate as well as precise, are to be obtained (Thompson and Wood, 1983). During the analysis, the diffractometer zero point and the specimen displacement error were allowed to refine freely. The specimen transparency correction was not allowed to vary but instead was included in the value expected from the calculated mass absorption coefficient and measured packing density of the sample. Beam divergences were fixed at the values calculated from the geometry of the diffractometer.

## 4. FT annealing in apatite: experiment and results

### 4.1. Annealing experiments

Annealing experiments were carried out on each apatite sample by measuring the reduction in full-length, neutron-induced tracks. Prior to irradiation, natural spontaneous tracks were removed by heating to 500 °C for 24 h; an aliquot of each annealed sample was then mounted, polished and etched to confirm total track erasure. Irradiation utilised the well-thermalised Risø reactor, Denmark (Cd ratio for Au>400), with neutron fluences between $7 \times 10^{15}$ and $2 \times 10^{16}$ n/cm$^2$, chosen according to each sample's uranium content, to provide sufficiently high track densities to facilitate analysis of adequate numbers of confined track lengths.

Laboratory annealing experiments used two identical Carbolite CSF 1100 muffle furnaces. Samples were wrapped in aluminium foil packets, placed in holes drilled in a preheated brass plate and inserted into an inner brass chamber (75 × 75 × 25 mm) within the furnace. Temperature was monitored in each furnace by five type-K thermocouples positioned between samples at a spacing of ~ 5–10 mm. Temperature was recorded every minute for each thermocouple throughout each experiment using a computer-controlled PICO TC-08 data logger. This configuration meant that each sample was monitored by two thermocouples. Fluctuation of temperatures recorded by an individual thermocouple never exceeded ± 1 °C, while maximum variation in temperatures monitored by different thermocouples was ± 3 °C.

Table 2
Fission-track annealing data measured for apatite BAM

| $t$ (h) | $T$ (°C) | Analyst #1 | | | | | | | Analyst #2 | | | | | | | Analyst #3 | | | | | | |
|---|---|---|---|---|---|---|---|---|---|---|---|---|---|---|---|---|---|---|---|---|---|---|
| | | $L$ (μm) | ± S.E. | ± S.D. | $N$ | $L/L_0$ | $A$ (°) | ± S.D. | $L$ (μm) | ± S.E. | ± S.D. | $N$ | $L/L_0$ | $A$ (°) | ± S.D. | $L$ (μm) | ± S.E. | ± S.D. | $N$ | $L/L_0$ | $A$ (°) | ± S.D. |
| 0 | | 16.57 | 0.11 | 1.06 | 100 | 1 | 51 | 22 | 16.34 | 0.10 | 0.99 | 103 | 1 | 54 | 23 | 16.67 | 0.09 | 0.86 | 101 | 1 | 48 | 21 |
| 10 | 200 | 15.40 | 0.09 | 0.92 | 100 | 0.929 | 55 | 22 | | | | | | | | 15.62 | 0.08 | 0.81 | 103 | 0.937 | 53 | 21 |
| 10 | 240 | 14.98 | 0.09 | 0.85 | 100 | 0.904 | 53 | 22 | 14.87 | 0.09 | 0.94 | 102 | 0.910 | 56 | 20 | 14.72 | 0.09 | 0.90 | 103 | 0.883 | 51 | 21 |
| 10 | 275 | 13.83 | 0.10 | 0.99 | 100 | 0.835 | 55 | 23 | 13.85 | 0.10 | 0.97 | 101 | 0.848 | 56 | 22 | 13.57 | 0.10 | 0.97 | 102 | 0.814 | 57 | 19 |
| 10 | 280 | 13.81 | 0.09 | 0.90 | 100 | 0.833 | 54 | 22 | 12.94 | 0.10 | 1.00 | 101 | 0.792 | 56 | 19 | 13.53 | 0.11 | 1.09 | 103 | 0.812 | 47 | 20 |
| 10 | 300 | 13.03 | 0.11 | 1.06 | 100 | 0.786 | 52 | 21 | 12.80 | 0.10 | 0.96 | 100 | 0.783 | 54 | 21 | 12.66 | 0.10 | 0.95 | 101 | 0.759 | 49 | 22 |
| 10 | 312 | 11.91 | 0.12 | 1.22 | 101 | 0.719 | 53 | 21 | 11.86 | 0.12 | 1.22 | 100 | 0.726 | 56 | 21 | 11.82 | 0.12 | 1.18 | 101 | 0.709 | 55 | 21 |
| 10 | 320 | 11.67 | 0.13 | 1.34 | 100 | 0.704 | 47 | 24 | 11.46 | 0.11 | 1.13 | 103 | 0.701 | 47 | 22 | 11.75 | 0.12 | 1.22 | 102 | 0.705 | 45 | 21 |
| 10 | 325 | 11.18 | 0.14 | 1.35 | 100 | 0.675 | 58 | 24 | 10.43 | 0.13 | 1.33 | 103 | 0.638 | 59 | 21 | 11.11 | 0.11 | 1.15 | 101 | 0.666 | 52 | 21 |
| 10 | 335 | 10.45 | 0.15 | 1.54 | 100 | 0.631 | 43 | 21 | | | | | | | | 10.08 | 0.19 | 1.89 | 101 | 0.605 | 46 | 23 |
| 10 | 345 | 9.71 | 0.25 | 1.95 | 63 | 0.586 | 33 | 15 | | | | | | | | 10.19 | 0.19 | 1.40 | 57 | 0.611 | 29 | 15 |
| 10 | 360 | track density too low | | | | | | | track density too low | | | | | | | track density too low | | | | | | |
| 100 | 210 | 14.92 | 0.09 | 0.93 | 100 | 0.900 | 48 | 24 | | | | | | | | 14.97 | 0.09 | 0.86 | 102 | 0.898 | 50 | 20 |
| 100 | 255 | 13.72 | 0.11 | 1.05 | 100 | 0.828 | 53 | 21 | | | | | | | | 13.79 | 0.09 | 0.94 | 101 | 0.827 | 50 | 21 |
| 100 | 275 | 12.69 | 0.09 | 0.91 | 100 | 0.766 | 46 | 21 | | | | | | | | 12.47 | 0.10 | 0.95 | 101 | 0.748 | 53 | 19 |
| 100 | 287 | 11.87 | 0.11 | 1.14 | 100 | 0.716 | 51 | 22 | | | | | | | | 11.97 | 0.10 | 1.03 | 102 | 0.718 | 51 | 23 |
| 100 | 295 | 11.27 | 0.13 | 1.26 | 100 | 0.680 | 51 | 22 | | | | | | | | 11.12 | 0.13 | 1.33 | 101 | 0.667 | 53 | 20 |

$t$ is the annealing time in hours and $T$ (°C) is the annealing temperature. $L$ is the arithmetic MTL. S.E. is the standard error of the mean. S.D. is the standard deviation of the sample. $N$ is the number of tracks measured and $A$ (°) is the arithmetic mean angle of tracks to the $c$-axis.
All samples etched in 5 M $HNO_3$ for 20 s at 20 ± 1 °C. Only TINTs measured. Data in italics have been acquired by using $^{252}Cf$ fission fragment irradiation (see Barbarand et al., 2003). $L = 0$ means no tracks can be seen in the sample; "track density too low" indicates that tracks can be seen but no MTL could be measured.

Table 3
Fission-track annealing data measured for apatite DRV

| $t$ (h) | $T$ (°C) | Analyst #1 | | | | | | | Analyst #2 | | | | | | | Analyst #3 | | | | | | |
|---|---|---|---|---|---|---|---|---|---|---|---|---|---|---|---|---|---|---|---|---|---|---|
| | | $L$ (μm) | ± S.E. | ± S.D. | $N$ | $L/L_0$ | $A$ (°) | ± S.D. | $L$ (μm) | ± S.E. | ± S.D. | $N$ | $L/L_0$ | $A$ (°) | ± S.D. | $L$ (μm) | ± S.E. | ± S.D. | $N$ | $L/L_0$ | $A$ (°) | ± S.D. |
| 0 | | 16.05 | 0.08 | 0.80 | 100 | 1 | 59 | 18 | 16.30 | 0.09 | 0.91 | 100 | 1 | 55 | 13 | 16.08 | 0.08 | 0.84 | 100 | 1 | 56 | 17 |
| 10 | 200 | 14.50 | 0.08 | 0.80 | 100 | 0.903 | 62 | 19 | | | | | | | | 15.07 | 0.08 | 0.81 | 100 | 0.937 | 60 | 15 |
| 10 | 240 | 13.72 | 0.07 | 0.71 | 101 | 0.855 | 61 | 18 | 13.96 | 0.08 | 0.85 | 103 | 0.856 | 56 | 17 | 14.11 | 0.09 | 0.85 | 101 | 0.877 | 61 | 17 |
| 10 | 275 | 12.45 | 0.11 | 1.11 | 100 | 0.776 | 60 | 18 | 12.44 | 0.08 | 0.78 | 103 | 0.763 | 60 | 17 | 12.57 | 0.08 | 0.83 | 102 | 0.782 | 57 | 17 |
| 10 | 280 | 11.43 | 0.11 | 1.11 | 100 | 0.712 | 61 | 16 | 12.05 | 0.09 | 0.88 | 103 | 0.739 | 57 | 16 | 11.72 | 0.10 | 0.98 | 103 | 0.729 | 58 | 16 |
| 10 | 300 | 9.91 | 0.14 | 1.37 | 100 | 0.617 | 54 | 17 | 9.66 | 0.15 | 1.48 | 102 | 0.593 | 52 | 17 | 9.68 | 0.20 | 2.01 | 102 | 0.602 | 54 | 17 |
| 10 | 312 | 6.50 | 0.28 | 2.79 | 100 | 0.405 | 42 | 16 | 6.97 | 0.20 | 1.99 | 101 | 0.428 | 38 | 14 | 5.92 | 0.29 | 2.93 | 101 | 0.368 | 41 | 16 |
| 10 | 320 | *7.36* | *0.23* | *2.27* | *100* | *0.459* | *24* | *14* | *7.28* | *0.21* | *2.14* | *101* | *0.447* | *29* | *16* | *6.01* | *0.35* | *2.63* | *57* | *0.374* | *32* | *10* |
| 10 | 325 | *6.39* | *0.22* | *2.23* | *100* | *0.398* | *21* | *16* | *6.36* | *0.21* | *2.08* | *101* | *0.390* | *22* | *12* | *7.23* | *0.21* | *2.08* | *100* | *0.450* | *18* | *11* |
| 10 | 335 | 0 | | | | | | | 0 | | | | | | | 0 | | | | | | |
| 100 | 210 | 14.09 | 0.09 | 0.87 | 100 | 0.878 | 62 | 17 | | | | | | | | 14.22 | 0.08 | 0.79 | 101 | 0.884 | 61 | 13 |
| 100 | 236 | | | | | | | | | | | | | | | 13.30 | 0.08 | 0.77 | 102 | 0.827 | | |
| 100 | 255 | 11.81 | 0.10 | 0.99 | 100 | 0.736 | 59 | 17 | | | | | | | | 11.95 | 0.09 | 0.88 | 100 | 0.743 | 58 | 17 |
| 100 | 275 | 9.51 | 0.14 | 1.44 | 100 | 0.593 | 48 | 15 | | | | | | | | 8.68 | 0.23 | 2.35 | 102 | 0.540 | 54 | 17 |
| 100 | 287 | 7.59 | 0.37 | 2.73 | 55 | 0.473 | 33 | 15 | | | | | | | | 5.67 | 0.30 | 3.06 | 101 | 0.353 | 37 | 16 |
| 100 | 295 | track density near zero | | | | | | | track density near zero | | | | | | | track density near zero | | | | | | |
| 1000 | 185 | 14.29 | 0.08 | 0.83 | 100 | 0.890 | 60 | 15 | | | | | | | | 14.49 | 0.08 | 0.77 | 100 | 0.901 | 62 | 13 |
| 1000 | 225 | 12.32 | 0.09 | 0.90 | 100 | 0.768 | 57 | 19 | | | | | | | | 12.45 | 0.08 | 0.81 | 101 | 0.774 | 59 | 14 |
| 1000 | 250 | 10.08 | 0.12 | 1.24 | 100 | 0.628 | 45 | 17 | | | | | | | | 9.17 | 0.21 | 2.15 | 101 | 0.570 | 48 | 16 |
| 1000 | 258 | | | | | | | | | | | | | | | 7.26 | 0.29 | 2.95 | 102 | 0.451 | 40 | 17 |
| 1000 | 266 | 7.39 | 0.26 | 2.56 | 100 | 0.460 | 23 | 14 | | | | | | | | 5.66 | 0.29 | 2.85 | 100 | 0.352 | 31 | 15 |

$t$ is the annealing time in hours and $T$ (°C) is the annealing temperature. $L$ is the arithmetic MTL. S.E. is the standard error of the mean. S.D. is the standard deviation of the sample. $N$ is the number of tracks measured and $A$ (°) is the arithmetic mean angle of tracks to the $c$-axis.
All samples etched in 5 M $HNO_3$ for 20 s at 20 ± 1 °C. Only TINTs measured. Data in italics have been acquired by using $^{252}Cf$ fission fragment irradiation (see Barbarand et al., 2003). $L = 0$ means no tracks can be seen in the sample; "track density too low" indicates that tracks can be seen but no MTL could be measured.

Table 4
Fission-track annealing data measured for apatite DUR

| $t$ (h) | $T$ (°C) | Analyst #1 | | | | | | | Analyst #2 | | | | | | | Analyst #3 | | | | | | |
|---|---|---|---|---|---|---|---|---|---|---|---|---|---|---|---|---|---|---|---|---|---|---|
| | | $L$ (μm) | ± S.E. | ± S.D. | $N$ | $L/L_0$ | $A$ (°) | ± S.D. | $L$ (μm) | ± S.E. | ± S.D. | $N$ | $L/L_0$ | $A$ (°) | ± S.D. | $L$ (μm) | ± S.E. | ± S.D. | $N$ | $L/L_0$ | $A$ (°) | ± S.D. |
| 0 | | 15.77 | 0.09 | 0.86 | 100 | 1 | 54 | 17 | 16.01 | (8) | 0.85 | 106 | 1 | 57 | 17 | 15.79 | (8) | 0.78 | 101 | 1 | 56 | 16 |
| 10 | 200 | 14.66 | 0.08 | 0.77 | 100 | 0.930 | 57 | 23 | | | | | | | | 14.98 | 0.08 | 0.80 | 101 | 0.949 | 56 | 15 |
| 10 | 235 | | | | | | | | | | | | | | | 14.26 | 0.08 | 0.75 | 101 | 0.903 | | |
| 10 | 240 | 14.07 | 0.09 | 0.85 | 100 | 0.892 | 61 | 17 | 14.06 | 0.07 | 0.78 | 113 | 0.878 | 58 | 17 | 14.16 | 0.07 | 0.69 | 101 | 0.897 | 57 | 16 |
| 10 | 275 | 12.64 | 0.08 | 0.79 | 100 | 0.802 | 63 | 19 | 13.22 | 0.09 | 0.91 | 105 | 0.826 | 54 | 20 | 12.34 | 0.09 | 0.89 | 100 | 0.782 | 58 | 18 |
| 10 | 280 | 12.71 | 0.11 | 1.05 | 100 | 0.806 | 57 | 18 | 11.94 | 0.09 | 0.92 | 103 | 0.746 | 57 | 14 | 12.57 | 0.09 | 0.95 | 103 | 0.796 | 59 | 16 |
| 10 | 300 | 11.18 | 0.11 | 1.05 | 100 | 0.709 | 56 | 23 | 11.01 | 0.11 | 1.13 | 101 | 0.688 | 58 | 20 | 11.09 | 0.07 | 0.74 | 102 | 0.702 | 60 | 17 |
| 10 | 310 | 10.28 | 0.11 | 1.09 | 100 | 0.652 | 56 | 21 | | | | | | | | 10.38 | 0.11 | 1.10 | 100 | 0.657 | 52 | 17 |
| 10 | 312 | 10.24 | 0.14 | 1.37 | 102 | 0.649 | 56 | 18 | 9.85 | 0.11 | 1.13 | 99 | 0.615 | 57 | 16 | 9.74 | 0.15 | 1.47 | 103 | 0.617 | 52 | 18 |
| 10 | 320 | 8.70 | 0.23 | 2.30 | 100 | 0.552 | 53 | 20 | 8.64 | 0.21 | 2.12 | 101 | 0.540 | 53 | 19 | 8.62 | 0.22 | 2.23 | 101 | 0.546 | 51 | 21 |
| 10 | 325 | 8.69 | 0.24 | 2.40 | 100 | 0.551 | 46 | 24 | 8.19 | 0.23 | 2.34 | 103 | 0.512 | 45 | 18 | 9.19 | 0.15 | 2.14 | 200 | 0.582 | 41 | 18 |
| 10 | 335 | track density near zero | | | | | | | track density near zero | | | | | | | track density near zero | | | | | | |
| 10 | 345 | 0 | | | | | | | 0 | | | | | | | 0 | | | | | | |
| 100 | 210 | 14.41 | 0.08 | 0.83 | 100 | 0.914 | 53 | 20 | | | | | | | | 14.48 | 0.08 | 0.81 | 102 | 0.917 | 57 | 18 |
| 100 | 255 | 13.13 | 0.08 | 0.80 | 100 | 0.833 | 51 | 22 | | | | | | | | 13.24 | 0.08 | 0.79 | 101 | 0.839 | 52 | 21 |
| 100 | 275 | 11.02 | 0.13 | 1.25 | 100 | 0.699 | 57 | 21 | | | | | | | | 10.81 | 0.10 | 1.02 | 101 | 0.685 | 56 | 19 |
| 100 | 287 | 10.34 | 0.11 | 1.12 | 102 | 0.656 | 50 | 21 | | | | | | | | 10.38 | 0.13 | 1.32 | 102 | 0.657 | 50 | 18 |
| 100 | 295 | 8.85 | 0.19 | 1.93 | 100 | 0.561 | 46 | 19 | | | | | | | | 8.45 | 0.25 | 2.52 | 102 | 0.535 | 48 | 19 |
| 1000 | 185 | 14.36 | 0.08 | 0.75 | 100 | 0.911 | 59 | 15 | | | | | | | | 14.51 | 0.06 | 0.65 | 102 | 0.919 | 56 | 15 |
| 1000 | 225 | 12.93 | 0.10 | 0.95 | 100 | 0.820 | 52 | 22 | | | | | | | | 12.99 | 0.08 | 0.82 | 102 | 0.823 | 55 | 17 |
| 1000 | 250 | 11.02 | 0.11 | 1.07 | 100 | 0.699 | 58 | 22 | | | | | | | | 10.84 | 0.11 | 1.11 | 102 | 0.687 | 53 | 21 |
| 1000 | 258 | | | | | | | | | | | | | | | 10.74 | 0.10 | 1.02 | 101 | 0.680 | 54 | 17 |
| 1000 | 266 | 9.71 | 0.16 | 1.55 | 100 | 0.616 | 49 | 21 | | | | | | | | 9.71 | 0.14 | 1.39 | 96 | 0.615 | 48 | 19 |

$t$ is the annealing time in hours and $T$ (°C) is the annealing temperature. $L$ is the arithmetic MTL. S.E. is the standard error of the mean. S.D. is the standard deviation of the sample. $N$ is the number of tracks measured and $A$ (°) is the arithmetic mean angle of tracks to the $c$-axis.
All samples etched in 5 M $HNO_3$ for 20 s at 20 ± 1 °C. Only TINTs measured. Data in italics have been acquired by using $^{252}Cf$ fission fragment irradiation (see Barbarand et al., 2003). $L = 0$ means no tracks can be seen in the sample; "track density too low" indicates that tracks can be seen but no MTL could be measured.

The homogeneity of temperature was further checked by simultaneously annealing five slices of Durango apatite at 300 °C for 10 h. The five pieces were placed at each corner and in the centre of the furnace annealing chamber, each piece separated from its neighbours by ~ 10–12 mm. Individual mean track lengths (MTLs) measured for the five apatite aliquots gave results indistinguishable within 1 standard error from the overall mean of 11.32 ± 0.08 μm and with no systematic variation in the chamber. This level of difference is equivalent to the analytical reproducibility determined on a single sample (see Barbarand et al., 2003), confirming that temperature is homogeneous within the furnace chamber and sample position in the furnace is not important.

Time–temperature conditions used for the annealing experiments were calculated from the results of Laslett et al. (1987) on Durango apatite and were selected to cover a range of mean track lengths, from 5 to 15 μm. Experimental heating times of 10, 100 and 1000 h were selected to enable comparison with previous studies (e.g. Crowley et al., 1991). Temperatures used ranged from 185 to 380 °C. Thermal equilibration following sample loading took 1–5 min according to the annealing experiment temperature. Such imprecision in time and temperature is considered insignificant within the total experimental time for long annealing experiments (10 h and greater), but may be a significant source of uncertainty for shorter annealing times. After each experiment, samples were removed and cooled on a heat sink to room temperature within a few seconds and thus cooling is not considered a significant source of error.

### 4.2. FT measurements

Apatite samples from each annealing experiment, together with control aliquots of full-length, unannealed, induced tracks were mounted and polished, and fission tracks etched for 20 s in 5 M $HNO_3$ at 20 ± 1 °C. Horizontal confined-track length measurement followed the procedures detailed in Barbarand et al. (2003). Only TINTs were measured throughout. Each sample was measured by two or three analysts. Variations between analysts exist and range between 0.1 μm for MTLs>14 μm to 0.35 μm for MTLs < 9 μm (see Barbarand et al., 2003 for discussion). The mean of the individual analyst determinations is presented throughout this study.

Table 5
Fission-track annealing data measured for apatite FAR

| *t* (h) | *T* (°C) | Analyst #1 | | | | | | Analyst #2 | | | | | | Analyst #3 | | | | | |
|---|---|---|---|---|---|---|---|---|---|---|---|---|---|---|---|---|---|---|---|
| | | *L* (μm) | ± S.E. | ± S.D. | *N* | A (°) | ± S.D. | *L* (μm) | ± S.E. | ± S.D. | *N* | A (°) | ± S.D. | *L* (μm) | ± S.E. | ± S.D. | *N* | A (°) | ± S.D. |
| 10 | 200 | 14.90 | 0.08 | 0.77 | 100 | 61 | 19 | | | | | | | 14.87 | 0.07 | 0.71 | 102 | 58 | 17 |
| 10 | 240 | 13.63 | 0.08 | 0.84 | 100 | 56 | 20 | | | | | | | 13.93 | 0.08 | 0.84 | 103 | 52 | 22 |
| 10 | 275 | 12.02 | 0.10 | 1.03 | 100 | 58 | 21 | 12.11 | 0.10 | 0.99 | 101 | 52 | 18 | 11.99 | 0.09 | 0.94 | 102 | 53 | 21 |
| 10 | 280 | 11.42 | 0.12 | 1.17 | 100 | 59 | 20 | | | | | | | 11.55 | 0.09 | 0.89 | 102 | 54 | 21 |
| 10 | 280 | | | | | | | | | | | | | 11.78 | 0.09 | 0.90 | 101 | 53 | 22 |
| 10 | 280 | | | | | | | | | | | | | 11.76 | 0.08 | 0.84 | 100 | 56 | 17 |
| 10 | 300 | 7.89 | 0.30 | 3.00 | 101 | 54 | 23 | 7.47 | 0.26 | 2.63 | 100 | 50 | 17 | 6.93 | 0.39 | 3.23 | 70 | 52 | 21 |
| 10 | 300 | | | | | | | | | | | | | 8.16 | 0.36 | 2.78 | 62 | 49 | 21 |
| 10 | 310 | *7.48* | *0.25* | *2.25* | *80* | *27* | *16* | | | | | | | *5.50* | *0.38* | *3.18* | *70* | *38* | *21* |
| 10 | 320 | track density near zero | | | | | | track density near zero | | | | | | track density near zero | | | | | |
| 10 | 325 | track density near zero | | | | | | track density near zero | | | | | | track density near zero | | | | | |
| 10 | 335 | 0 | | | | | | 0 | | | | | | 0 | | | | | |
| 100 | 210 | 14.01 | 0.08 | 0.80 | 100 | 57 | 22 | | | | | | | 14.18 | 0.07 | 0.75 | 110 | 55 | 18 |
| 100 | 295 | track density near zero | | | | | | track density near zero | | | | | | track density near zero | | | | | |

*t* is the annealing time in hours and *T* (°C) is the annealing temperature. *L* is the arithmetic MTL. S.E. is the standard error of the mean. S.D. is the standard deviation of the sample. *N* is the number of tracks measured and *A* (°) is the arithmetic mean angle of tracks to the *c*-axis.
All samples etched in 5 M $HNO_3$ for 20 s at 20 ± 1 °C. Only TINTs measured. Data in italics have been acquired by using $^{252}Cf$ fission fragment irradiation (see Barbarand et al., 2003). *L* = 0 means no tracks can be seen in the sample; "track density too low" indicates that tracks can be seen but no MTL could be measured.

### 4.3. Annealing results

The measured track-length data are presented in Tables 2–14 for each sample and heating step. Fig. 2 plots the results for the 10-, 100- and 1000-h annealing experiments and shows that FT lengths in the 13 compositionally different apatites have been shortened by different amounts for the same temperature step. These variations are significant, systematic and comparable to previous studies (e.g. Carlson et al., 1999). Small but significant differences exist between samples at low levels of annealing but these differences increase with temperature. The relative response of each apatite remains the same for each of our experiments (10, 100 and 1000 h) such that GUN is always the most resistant to annealing and FAR is the least resistant. In order of resistance to annealing, we observe the trend GUN, LIN, FCT, BAM, FUL, UMB, MIN, DUR, GIL, DRV, WIL, UNK and FAR. Two of the apatite samples (DUR and FCT) have already been studied by Carlson et al. (1999) and results for each apatite show good agreement between the two studies.

## 5. Apatite unit cell and annealing response

### 5.1. Correlation

The results of these annealing experiments reinforce the observation that apatite composition has an important control on fission-track annealing rate. This control represents the summed affects of the type and amount of elemental substitution, linked together with the substitution sites. These factors directly affect the apatite unit cell and hence the cell parameters should also display a relationship with FT annealing rate.

Fig. 3 plots unit-cell parameters $a$ and $c$ against fission-track MTL measured for 10 of the apatite

Table 6
Fission-track annealing data measured for apatite FCT

| $t$ (h) | $T$ (°C) | Analyst #1 | | | | | | | Analyst #3 | | | | | | |
|---|---|---|---|---|---|---|---|---|---|---|---|---|---|---|---|
| | | $L$ (μm) | ± S.E. | ± S.D. | $N$ | L/$L_0$ | $A$ (°) | ± S.D. | $L$ (μm) | ± S.E. | ± S.D. | $N$ | L/$L_0$ | $A$ (°) | ± S.D. |
| 0 | | 15.75 | 0.09 | 0.87 | 100 | 1 | 59 | 21 | 15.80 | 0.07 | 0.73 | 99 | 1 | 60 | 19 |
| 10 | 200 | 14.88 | 0.07 | 0.74 | 101 | 0.945 | 55 | 20 | 15.20 | 0.08 | 0.82 | 102 | 0.962 | 58 | 18 |
| 10 | 230 | 14.59 | 0.08 | 0.78 | 100 | 0.926 | 59 | 19 | 14.68 | 0.07 | 0.74 | 101 | 0.929 | 56 | 20 |
| 10 | 270 | 13.97 | 0.09 | 0.85 | 100 | 0.887 | 58 | 19 | 14.21 | 0.08 | 0.8 | 101 | 0.899 | | |
| 10 | 280 | 13.74 | 0.08 | 0.82 | 100 | 0.872 | 58 | 20 | 13.63 | 0.09 | 0.87 | 101 | 0.863 | 56 | 19 |
| 10 | 295 | 13.08 | 0.08 | 0.83 | 100 | 0.830 | 54 | 19 | 13.10 | 0.07 | 0.68 | 102 | 0.829 | 55 | 22 |
| 10 | 310 | 12.19 | 0.08 | 0.83 | 100 | 0.774 | 56 | 19 | 12.22 | 0.08 | 0.83 | 102 | 0.773 | 58 | 19 |
| 10 | 320 | 11.42 | 0.11 | 1.09 | 100 | 0.725 | 56 | 16 | 11.47 | 0.11 | 1.07 | 102 | 0.726 | 57 | 20 |
| 10 | 325 | 10.90 | 0.09 | 0.86 | 100 | 0.692 | 56 | 19 | 11.11 | 0.10 | 1.01 | 102 | 0.703 | | |
| 10 | 335 | 9.26 | 0.13 | 1.13 | 76 | 0.588 | 52 | 21 | 8.15 | 0.23 | 2.09 | 84 | 0.516 | 56 | 21 |
| 10 | 345 | *7.84* | *0.24* | *2.46* | *102* | *0.498* | *36* | *18* | *6.73* | *0.28* | *2.84* | *100* | *0.426* | *39* | *21* |
| 10 | 360 | track density too low | | | | | | | track density too low | | | | | | |
| 100 | 210 | 14.49 | 0.08 | 0.83 | 100 | 0.920 | 56 | 20 | 14.70 | 0.09 | 0.85 | 101 | 0.930 | 56 | 23 |
| 100 | 255 | 13.19 | 0.10 | 0.99 | 100 | 0.837 | 57 | 19 | 13.55 | 0.07 | 0.66 | 102 | 0.858 | 53 | 17 |
| 100 | 275 | 12.70 | 0.09 | 0.86 | 100 | 0.806 | 58 | 21 | 12.73 | 0.09 | 0.88 | 103 | 0.806 | 53 | 20 |
| 100 | 295 | 11.02 | 0.09 | 0.96 | 110 | 0.700 | 57 | 17 | 11.00 | 0.11 | 1.09 | 103 | 0.696 | 55 | 21 |
| 1000 | 185 | 14.73 | 0.09 | 0.89 | 101 | 0.935 | 58 | 18 | 14.80 | 0.08 | 0.78 | 103 | 0.937 | 57 | 19 |
| 1000 | 225 | 13.74 | 0.09 | 0.91 | 100 | 0.872 | 56 | 21 | 13.82 | 0.09 | 0.85 | 102 | 0.875 | 54 | 18 |
| 1000 | 250 | 12.71 | 0.09 | 0.95 | 103 | 0.807 | 57 | 20 | 12.86 | 0.08 | 0.82 | 102 | 0.814 | 52 | 20 |
| 1000 | 258 | | | | | | | | 12.00 | 0.11 | 1.10 | 101 | 0.759 | 59 | 18 |
| 1000 | 266 | 11.65 | 0.10 | 1.00 | 100 | 0.737 | 58 | 18 | 11.81 | 0.09 | 0.93 | 104 | 0.747 | 51 | 21 |
| 1000 | 275 | | | | | | | | 10.54 | 0.11 | 1.06 | 101 | 0.667 | 55 | 21 |

$t$ is the annealing time in hours and $T$ (°C) is the annealing temperature. $L$ is the arithmetic MTL. S.E. is the standard error of the mean. S.D. is the standard deviation of the sample. $N$ is the number of tracks measured and $A$ (°) is the arithmetic mean angle of tracks to the $c$-axis. All samples etched in 5 M $HNO_3$ for 20 s at 20 ± 1 °C. Only TINTs measured. Data in italics have been acquired by using $^{252}Cf$ fission fragment irradiation (see Barbarand et al., 2003). $L = 0$ means no tracks can be seen in the sample; "track density too low" indicates that tracks can be seen but no MTL could be measured.

Table 7
Fission-track annealing data measured for apatite FUL

| $t$ (h) | $T$ (°C) | Analyst #1 | | | | | | | Analyst #2 | | | | | | | Analyst #3 | | | | | | |
|---|---|---|---|---|---|---|---|---|---|---|---|---|---|---|---|---|---|---|---|---|---|---|
| | | $L$ (μm) | ± S.E. | ± S.D. | $N$ | $L/L_0$ | $A$ (°) | ± S.D. | $L$ (μm) | ± S.E. | ± S.D. | $N$ | $L/L_0$ | $A$ (°) | ± S.D. | $L$ (μm) | ± S.E. | ± S.D. | $N$ | $L/L_0$ | $A$ (°) | ± S.D. |
| 0 | | 16.05 | 0.11 | 0.79 | 55 | 1 | 54 | 22 | 15.98 | 0.09 | 0.89 | 104 | 1 | 56 | 23 | 15.96 | 0.14 | 0.89 | 42 | 1 | 56 | 22 |
| 10 | 200 | 15.02 | 0.08 | 0.81 | 100 | 0.936 | 57 | 21 | | | | | | | | 15.07 | 0.08 | 0.77 | 102 | 0.944 | 57 | 18 |
| 10 | 275 | 13.36 | 0.08 | 0.84 | 100 | 0.832 | 60 | 23 | 13.69 | 0.09 | 0.90 | 103 | 0.857 | 61 | 15 | 13.30 | 0.06 | 0.65 | 101 | 0.833 | 59 | 15 |
| 10 | 280 | 13.86 | 0.09 | 0.93 | 100 | 0.864 | 55 | 19 | 13.44 | 0.08 | 0.84 | 107 | 0.841 | 60 | 20 | 13.86 | 0.07 | 0.75 | 104 | 0.868 | 54 | 19 |
| 10 | 290 | 13.25 | 0.08 | 0.79 | 100 | 0.826 | 52 | 21 | | | | | | | | 13.12 | 0.07 | 0.75 | 102 | 0.822 | 57 | 14 |
| 10 | 300 | 12.55 | 0.09 | 0.85 | 100 | 0.782 | 55 | 21 | 12.42 | 0.09 | 0.87 | 104 | 0.777 | 56 | 17 | 12.67 | 0.08 | 0.83 | 102 | 0.794 | 55 | 18 |
| 10 | 312 | 10.69 | 0.26 | 1.52 | 34 | 0.666 | 47 | 26 | 9.90 | 0.29 | 0.87 | 10 | 0.620 | 60 | 20 | 10.98 | 0.27 | 0.94 | 13 | 0.688 | 48 | 21 |
| 10 | 320 | 11.03 | 0.11 | 1.11 | 100 | 0.687 | 57 | 20 | | | | | | | | 11.07 | 0.09 | 0.89 | 102 | 0.694 | 57 | 18 |
| 10 | 335 | *7.37* | *0.26* | *2.64* | *101* | *0.459* | *34* | *21* | | | | | | | | *6.75* | *0.28* | *2.80* | *102* | *0.423* | *57* | *19* |
| 10 | 345 | 6.41 | 0.71 | 3.53 | 25 | 0.399 | 47 | 25 | | | | | | | | 5.43 | 0.59 | 3.28 | 31 | 0.340 | 53 | 22 |
| 100 | 210 | 14.37 | 0.08 | 0.83 | 100 | 0.895 | 59 | 20 | | | | | | | | 14.71 | 0.08 | 0.76 | 101 | 0.922 | 33 | 20 |
| 100 | 255 | 13.60 | 0.09 | 0.89 | 100 | 0.847 | 53 | 22 | | | | | | | | 13.64 | 0.08 | 0.84 | 102 | 0.855 | 54 | 20 |
| 100 | 275 | 12.36 | 0.08 | 0.77 | 100 | 0.770 | 60 | 18 | | | | | | | | 12.57 | 0.07 | 0.73 | 103 | 0.788 | 58 | 17 |
| 100 | 287 | 11.73 | 0.09 | 0.94 | 100 | 0.731 | 55 | 22 | | | | | | | | 11.72 | 0.09 | 0.92 | 103 | 0.734 | 56 | 20 |
| 100 | 295 | 10.67 | 0.11 | 1.05 | 100 | 0.665 | 53 | 20 | | | | | | | | 10.42 | 0.10 | 0.96 | 102 | 0.653 | 58 | 18 |
| 1000 | 185 | 14.47 | 0.09 | 0.90 | 100 | 0.902 | 59 | 18 | | | | | | | | 14.75 | 0.08 | 0.75 | 101 | 0.924 | 60 | 18 |
| 1000 | 225 | 13.63 | 0.09 | 0.90 | 100 | 0.849 | 57 | 22 | | | | | | | | 13.36 | 0.08 | 0.80 | 103 | 0.837 | 57 | 18 |
| 1000 | 250 | 12.48 | 0.10 | 0.98 | 100 | 0.778 | 58 | 22 | | | | | | | | 12.40 | 0.08 | 0.82 | 103 | 0.777 | 51 | 21 |
| 1000 | 266 | 11.32 | 0.09 | 0.92 | 100 | 0.705 | 57 | 19 | | | | | | | | 11.74 | 0.09 | 0.89 | 102 | 0.736 | 55 | 19 |
| 1000 | 275 | | | | | | | | | | | | | | | 10.19 | 0.12 | 1.19 | 101 | 0.638 | 54 | 18 |

$t$ is the annealing time in hours and $T$ (°C) is the annealing temperature. $L$ is the arithmetic MTL. S.E. is the standard error of the mean. S.D. is the standard deviation of the sample. $N$ is the number of tracks measured and $A$ (°) is the arithmetic mean angle of tracks to the $c$-axis.
All samples etched in 5 M $HNO_3$ for 20 s at 20 ± 1 °C. Only TINTs measured. Data in italics have been acquired by using $^{252}Cf$ fission fragment irradiation (see Barbarand et al., 2003). $L = 0$ means no tracks can be seen in the sample; ''track density too low'' indicates that tracks can be seen but no MTL could be measured.

Table 8
Fission-track annealing data measured for apatite GIL

| $t$ (h) | $T$ (°C) | Analyst #1 | | | | | | | Analyst #2 | | | | | | | Analyst #3 | | | | | | |
|---|---|---|---|---|---|---|---|---|---|---|---|---|---|---|---|---|---|---|---|---|---|---|
| | | $L$ (μm) | ± S.E. | ± S.D. | $N$ | $L/L_0$ | $A$ (°) | ± S.D. | $L$ (μm) | ± S.E. | ± S.D. | $N$ | $L/L_0$ | $A$ (°) | ± S.D. | $L$ (μm) | ± S.E. | ± S.D. | $N$ | $L/L_0$ | $A$ (°) | ± S.D. |
| 0 | | 16.23 | 0.10 | 0.95 | 100 | 1 | 61 | 22 | 16.30 | (8) | 0.79 | 105 | 1 | 61 | 22 | 16.06 | 0.07 | 0.71 | 101 | 1 | 57 | 24 |
| 10 | 200 | 14.98 | 0.09 | 0.89 | 100 | 0.923 | 57 | 23 | | | | | | | | 15.18 | 0.09 | 0.87 | 101 | 0.945 | 60 | 20 |
| 10 | 240 | 14.02 | 0.09 | 0.86 | 100 | 0.864 | 61 | 22 | 13.97 | (10) | 0.95 | 96 | 0.857 | 58 | 22 | 14.03 | 0.07 | 0.74 | 102 | 0.874 | 52 | 23 |
| 10 | 275 | 12.44 | 0.10 | 0.97 | 100 | 0.766 | 62 | 21 | 12.31 | (8) | 0.78 | 104 | 0.755 | 63 | 19 | 12.42 | 0.09 | 0.93 | 103 | 0.773 | 61 | 20 |
| 10 | 280 | 12.06 | 0.10 | 1.00 | 100 | 0.743 | 56 | 22 | 12.08 | (8) | 0.82 | 104 | 0.741 | 57 | 19 | 12.12 | 0.08 | 0.81 | 101 | 0.755 | 63 | 18 |
| 10 | 300 | 9.61 | 0.18 | 1.78 | 100 | 0.592 | 56 | 22 | 9.90 | (13) | 1.30 | 102 | 0.607 | 53 | 21 | 9.75 | 0.14 | 1.46 | 103 | 0.607 | 56 | 22 |
| 10 | 312 | *7.51* | *0.26* | *2.62* | *100* | *0.463* | *31* | *21* | *6.69* | *(24)* | *2.40* | *103* | *0.410* | *34* | *23* | *6.23* | *0.28* | *2.8* | *101* | *0.388* | *38* | *22* |
| 10 | 320 | *7.71* | *0.58* | *1.41* | *7* | *0.475* | | | | | | | | | | *7.79* | *0.24* | *1.57* | *43* | *0.485* | *13* | *8* |
| 10 | 325 | *6.38* | *0.27* | *1.60* | *35* | *0.393* | *9* | *10* | | | | | | | | *5.86* | *1.24* | *2.2* | *4* | *0.365* | | |
| 10 | 335 | 0 | | | | | | | 0 | | | | | | | 0 | | | | | | |
| 100 | 210 | 14.34 | 0.09 | 0.94 | 100 | 0.884 | 59 | 24 | | | | | | | | 14.29 | 0.08 | 0.82 | 100 | 0.890 | 58 | 21 |
| 100 | 255 | 12.10 | 0.09 | 0.92 | 100 | 0.746 | 62 | 21 | | | | | | | | 12.28 | 0.08 | 0.84 | 102 | 0.765 | 55 | 22 |
| 100 | 275 | 9.65 | 0.12 | 1.20 | 100 | 0.595 | 57 | 20 | | | | | | | | 10.01 | 0.13 | 1.32 | 103 | 0.623 | 49 | 21 |
| 100 | 287 | *8.56* | *0.21* | *2.05* | *100* | *0.527* | *19* | *14* | | | | | | | | *8.20* | *0.24* | *1.99* | *69* | *0.511* | *21* | *16* |
| 100 | 295 | track density too low | | | | | | | | | | | | | | track density too low | | | | | | |
| 1000 | 185 | 14.26 | 0.08 | 0.77 | 100 | 0.879 | 59 | 21 | | | | | | | | 14.60 | 0.07 | 0.73 | 103 | 0.909 | 56 | 21 |
| 1000 | 225 | 12.59 | 0.09 | 0.90 | 100 | 0.776 | 63 | 19 | | | | | | | | 12.66 | 0.09 | 0.93 | 102 | 0.788 | 56 | 20 |
| 1000 | 250 | 9.83 | 0.13 | 1.30 | 100 | 0.606 | 50 | 22 | | | | | | | | 9.80 | 0.17 | 1.69 | 102 | 0.610 | 49 | 23 |
| 1000 | 266 | track density too low | | | | | | | | | | | | | | track density too low | | | | | | |
| 1000 | 275 | 0 | | | | | | | 0 | | | | | | | 0 | | | | | | |

$t$ is the annealing time in hours and $T$ (°C) is the annealing temperature. $L$ is the arithmetic MTL. S.E. is the standard error of the mean. S.D. is the standard deviation of the sample. $N$ is the number of tracks measured and $A$ (°) is the arithmetic mean angle of tracks to the $c$-axis.
All samples etched in 5 M $HNO_3$ for 20 s at 20 ± 1 °C. Only TINTs measured. Data in italics have been acquired by using $^{252}Cf$ fission fragment irradiation (see Barbarand et al., 2003). $L = 0$ means no tracks can be seen in the sample; "track density too low" indicates that tracks can be seen but no MTL could be measured.

Table 9
Fission-track annealing data measured for apatite GUN

| $t$ (h) | $T$ (°C) | Analyst #1 | | | | | | | Analyst #2 | | | | | | | Analyst #3 | | | | | | |
|---|---|---|---|---|---|---|---|---|---|---|---|---|---|---|---|---|---|---|---|---|---|---|
| | | $L$ (μm) | ± S.E. | ± S.D. | $N$ | $L/L_0$ | $A$ (°) | ± S.D. | $L$ (μm) | ± S.E. | ± S.D. | $N$ | $L/L_0$ | $A$ (°) | ± S.D. | $L$ (μm) | ± S.E. | ± S.D. | $N$ | $L/L_0$ | $A$ (°) | ± S.D. |
| 0 | | 16.71 | 0.09 | 0.93 | 100 | 1 | 56 | 22 | | | | | | | | 16.53 | 0.10 | 0.97 | 101 | 1 | 55 | 21 |
| 10 | 280 | 14.50 | 0.10 | 0.98 | 100 | 0.868 | 53 | 22 | | | | | | | | 14.46 | 0.07 | 0.72 | 102 | 0.875 | 52 | 21 |
| 10 | 290 | 14.33 | 0.08 | 0.76 | 100 | 0.858 | 56 | 22 | | | | | | | | 14.23 | 0.08 | 0.82 | 104 | 0.861 | 52 | 21 |
| 10 | 300 | 13.18 | 0.08 | 0.82 | 100 | 0.789 | 56 | 21 | 13.07 | 0.11 | 1.09 | 101 | 0.782 | 61 | 18 | 13.49 | 0.08 | 0.83 | 102 | 0.816 | 53 | 21 |
| 10 | 320 | *12.65* | *0.10* | *0.99* | *100* | *0.757* | *58* | *20* | *12.64* | *0.09* | *0.91* | *104* | *0.756* | *57* | *20* | *12.71* | *0.09* | *0.87* | *102* | *0.769* | *54* | *20* |
| 10 | 325 | 12.89 | 0.11 | 1.06 | 100 | 0.771 | 55 | 22 | | | | | | | | 12.73 | 0.08 | 0.82 | 102 | 0.770 | 55 | 21 |
| 10 | 335 | 12.18 | 0.09 | 0.86 | 100 | 0.729 | 55 | 20 | | | | | | | | 12.15 | 0.09 | 0.95 | 101 | 0.735 | 55 | 20 |
| 10 | 345 | 10.99 | 0.10 | 1.00 | 100 | 0.658 | 53 | 22 | | | | | | | | 10.87 | 0.12 | 1.17 | 101 | 0.658 | 53 | 21 |
| 10 | 350 | 10.62 | 0.11 | 1.14 | 100 | 0.636 | | | | | | | | | | 10.41 | 0.10 | 1.04 | 102 | 0.630 | 52 | 20 |
| 10 | 360 | 8.77 | 0.20 | 2.02 | 100 | 0.525 | 46 | 24 | | | | | | | | 8.20 | 0.23 | 2.44 | 109 | 0.496 | 48 | 23 |
| 10 | 370 | track density near zero | | | | | | | | | | | | | | track density near zero | | | | | | |
| 1000 | 185 | 15.05 | 0.08 | 0.80 | 100 | 0.901 | 58 | 19 | | | | | | | | 15.59 | 0.08 | 0.82 | 101 | 0.943 | 48 | 22 |
| 1000 | 225 | 14.27 | 0.09 | 0.95 | 121 | 0.854 | 55 | 19 | | | | | | | | 14.53 | 0.07 | 0.73 | 102 | 0.879 | 53 | 20 |
| 1000 | 250 | 13.81 | 0.09 | 0.92 | 100 | 0.826 | 55 | 20 | | | | | | | | 14.01 | 0.09 | 0.93 | 103 | 0.848 | 52 | 23 |
| 1000 | 266 | 13.20 | 0.07 | 0.82 | 137 | 0.790 | 54 | 20 | | | | | | | | 13.27 | 0.09 | 0.89 | 102 | 0.803 | 51 | 21 |
| 1000 | 275 | | | | | | | | | | | | | | | 12.77 | 0.09 | 0.90 | 104 | 0.773 | 55 | 21 |

$t$ is the annealing time in hours and $T$ (°C) is the annealing temperature. $L$ is the arithmetic MTL. S.E. is the standard error of the mean. S.D. is the standard deviation of the sample. $N$ is the number of tracks measured and $A$ (°) is the arithmetic mean angle of tracks to the $c$-axis.
All samples etched in 5 M $HNO_3$ for 20 s at 20 ± 1 °C. Only TINTs measured. Data in italics have been acquired by using $^{252}Cf$ fission fragment irradiation (see Barbarand et al., 2003). $L = 0$ means no tracks can be seen in the sample; "track density too low" indicates that tracks can be seen but no MTL could be measured.

Table 10
Fission-track annealing data measured for apatite LIN

| $t$ (h) | $T$ (°C) | Analyst #1 | | | | | | | Analyst #2 | | | | | | | Analyst #3 | | | | | | |
|---|---|---|---|---|---|---|---|---|---|---|---|---|---|---|---|---|---|---|---|---|---|---|
| | | $L$ (μm) | ± S.E. | ± S.D. | $N$ | $L/L_0$ | $A$ (°) | ± S.D. | $L$ (μm) | ± S.E. | ± S.D. | $N$ | $L/L_0$ | $A$ (°) | ± S.D. | $L$ (μm) | ± S.E. | ± S.D. | $N$ | $L/L_0$ | $A$ (°) | ± S.D. |
| 0 | | 16.28 | 0.09 | 0.87 | 100 | 1 | 56 | 22 | | | | | | | | 16.35 | 0.08 | 0.80 | 100 | 1 | 53 | 23 |
| 10 | 275 | 13.83 | 0.13 | 0.99 | 56 | 0.850 | 59 | 19 | 13.86 | 0.13 | 0.9 | 43 | 0.851 | 51 | 23 | 13.99 | 0.21 | 1.02 | 24 | 0.856 | 52 | 20 |
| 10 | 280 | 13.87 | 0.12 | 1.16 | 100 | 0.852 | 59 | 20 | | | | | | | | 13.84 | 0.14 | 1.21 | 79 | 0.846 | 60 | 20 |
| 10 | 300 | 13.23 | 0.13 | 1.30 | 100 | 0.813 | 55 | 18 | | | | | | | | 13.47 | 0.10 | 0.95 | 100 | 0.824 | 52 | 21 |
| 10 | 310 | 12.69 | 0.14 | 1.37 | 100 | 0.779 | 53 | 25 | 12.68 | 0.11 | 1.1 | 100 | 0.779 | 58 | 21 | 13.13 | 0.10 | 1.04 | 100 | 0.803 | 53 | 23 |
| 10 | 320 | 11.98 | 0.15 | 1.40 | 86 | 0.736 | 55 | 21 | | | | | | | | 11.53 | 0.21 | 1.71 | 68 | 0.705 | 55 | 21 |
| 10 | 335 | 10.10 | 0.34 | 1.5 | 19 | 0.618 | 63 | 17 | | | | | | | | | | | | | | |
| 10 | 335 | *10.51* | *0.20* | *1.98* | *100* | *0.643* | *58* | *22* | | | | | | | | *10.26* | *0.20* | *1.99* | *101* | *0.628* | *59* | *20* |
| 10 | 345 | 9.38 | 0.39 | 2.64 | 46 | 0.576 | 55 | 24 | | | | | | | | 7.71 | 0.52 | 2.74 | 28 | 0.472 | 56 | 23 |
| 10 | 360 | track density too low | | | | | | | track density too low | | | | | | | track density too low | | | | | | |
| 100 | 210 | 14.93 | 0.14 | 1.40 | 100 | 0.917 | 58 | 20 | | | | | | | | 14.82 | 0.15 | 1.41 | 85 | 0.906 | 55 | 22 |
| 100 | 295 | 11.98 | 0.15 | 1.50 | 100 | 0.736 | 56 | 21 | | | | | | | | 12.21 | 0.15 | 1.29 | 79 | 0.747 | 60 | 22 |
| 1000 | 185 | 14.67 | 0.10 | 0.93 | 81 | 0.897 | 60 | 23 | | | | | | | | 14.74 | 0.14 | 1.21 | 72 | 0.902 | 53 | 22 |
| 1000 | 225 | 13.92 | 0.09 | 0.94 | 100 | 0.851 | 60 | 21 | | | | | | | | 13.98 | 0.10 | 0.73 | 55 | 0.855 | 56 | 23 |
| 1000 | 250 | 12.83 | 0.15 | 1.35 | 86 | 0.785 | 59 | 21 | | | | | | | | 12.76 | 0.20 | 1.46 | 56 | 0.780 | 59 | 22 |
| 1000 | 266 | 12.71 | 0.15 | 1.01 | 45 | 0.777 | 59 | 18 | | | | | | | | 12.51 | 0.20 | 1.42 | 52 | 0.765 | 55 | 20 |

$t$ is the annealing time in hours and $T$ (°C) is the annealing temperature. $L$ is the arithmetic MTL. S.E. is the standard error of the mean. S.D. is the standard deviation of the sample. $N$ is the number of tracks measured and $A$ (°) is the arithmetic mean angle of tracks to the $c$-axis.
All samples etched in 5 M $HNO_3$ for 20 s at 20 ± 1 °C. Only TINTs measured. Data in italics have been acquired by using $^{252}Cf$ fission fragment irradiation (see Barbarand et al., 2003). $L = 0$ means no tracks can be seen in the sample; "track density too low" indicates that tracks can be seen but no MTL could be measured.

Table 11
Fission-track annealing data measured for apatite MIN

| $t$ (h) | $T$ (°C) | Analyst #1 | | | | | | | Analyst #2 | | | | | | | Analyst #3 | | | | | | |
|---|---|---|---|---|---|---|---|---|---|---|---|---|---|---|---|---|---|---|---|---|---|---|
| | | $L$ (μm) | ± S.E. | ± S.D. | $N$ | $L/L_0$ | $A$ (°) | ± S.D. | $L$ (μm) | ± S.E. | ± S.D. | $N$ | $L/L_0$ | $A$ (°) | ± S.D. | $L$ (μm) | ± S.E. | ± S.D. | $N$ | $L/L_0$ | $A$ (°) | ± S.D. |
| 0 | | 16.20 | 0.09 | 0.90 | 100 | 1 | 57 | 18 | 16.12 | 0.10 | 1.00 | 108 | 1 | 62 | 17 | 16.33 | 0.09 | 0.93 | 102 | 1 | 55 | 17 |
| 10 | 200 | 15.10 | 0.10 | 0.95 | 100 | 0.932 | 57 | 24 | | | | | | | | 15.17 | 0.08 | 0.83 | 102 | 0.929 | 58 | 18 |
| 10 | 240 | 14.22 | 0.09 | 0.90 | 100 | 0.878 | 60 | 20 | 14.39 | 0.09 | 0.88 | 102 | 0.893 | 58 | 19 | 14.50 | 0.07 | 0.68 | 103 | 0.888 | 55 | 19 |
| 10 | 275 | 12.80 | 0.10 | 1.02 | 100 | 0.790 | 59 | 19 | 12.59 | 0.10 | 1.06 | 103 | 0.781 | 56 | 20 | 12.38 | 0.13 | 1.25 | 95 | 0.758 | 47 | 18 |
| 10 | 280 | 12.88 | 0.10 | 1.03 | 100 | 0.795 | 59 | 23 | 12.70 | 0.08 | 0.83 | 103 | 0.788 | 58 | 15 | 12.55 | 0.08 | 0.85 | 102 | 0.769 | 58 | 15 |
| 10 | 300 | 11.81 | 0.10 | 0.96 | 100 | 0.729 | 61 | 19 | 11.74 | 0.09 | 0.90 | 102 | 0.728 | 56 | 19 | 11.69 | 0.09 | 0.93 | 102 | 0.716 | 56 | 18 |
| 10 | 312 | 9.89 | 0.18 | 1.82 | 100 | 0.610 | 58 | 18 | | | | | | | | 10.40 | 0.11 | 1.07 | 103 | 0.637 | 48 | 18 |
| 10 | 320 | 8.10 | 0.25 | 2.49 | 100 | 0.500 | 51 | 21 | | | | | | | | 8.18 | 0.26 | 2.62 | 102 | 0.501 | 45 | 18 |
| 10 | 325 | 8.44 | 0.22 | 2.23 | 100 | 0.521 | 46 | 20 | | | | | | | | 8.21 | 0.24 | 2.46 | 103 | 0.503 | 46 | 19 |
| 10 | 335 | track density near zero | | | | | | | track density near zero | | | | | | | track density near zero | | | | | | |
| 10 | 345 | 0 | | | | | | | 0 | | | | | | | 0 | | | | | | |
| 100 | 210 | 14.51 | 0.08 | 0.81 | 100 | 0.896 | 58 | 20 | | | | | | | | 14.76 | 0.09 | 0.87 | 100 | 0.904 | 57 | 19 |
| 100 | 255 | 13.22 | 0.09 | 0.89 | 100 | 0.816 | 54 | 18 | | | | | | | | 13.13 | 0.08 | 0.83 | 102 | 0.804 | 53 | 17 |
| 100 | 275 | 11.68 | 0.11 | 1.13 | 100 | 0.721 | 51 | 19 | | | | | | | | 11.80 | 0.10 | 0.98 | 101 | 0.723 | 47 | 19 |
| 100 | 287 | 10.16 | 0.14 | 1.41 | 100 | 0.627 | 50 | 21 | | | | | | | | 10.05 | 0.12 | 1.16 | 102 | 0.615 | 50 | 18 |
| 100 | 295 | 8.83 | 0.21 | 2.09 | 100 | 0.545 | 40 | 17 | | | | | | | | 8.14 | 0.18 | 2.58 | 200 | 0.498 | 44 | 19 |
| 1000 | 185 | 14.59 | 0.07 | 0.72 | 100 | 0.901 | 60 | 18 | | | | | | | | 14.86 | 0.08 | 0.80 | 101 | 0.910 | 53 | 19 |
| 1000 | 225 | 13.52 | 0.09 | 0.91 | 100 | 0.835 | 55 | 19 | | | | | | | | 13.68 | 0.10 | 0.99 | 107 | 0.838 | 52 | 20 |
| 1000 | 250 | 11.80 | 0.10 | 1.02 | 100 | 0.728 | 53 | 22 | | | | | | | | 11.96 | 0.09 | 0.94 | 102 | 0.732 | 52 | 19 |
| 1000 | 266 | 9.49 | 0.18 | 1.82 | 101 | 0.586 | 47 | 20 | | | | | | | | 9.54 | 0.16 | 1.59 | 102 | 0.584 | 52 | 17 |
| 1000 | 275 | | | | | | | | | | | | | | | 6.72 | 0.26 | 2.61 | 101 | 0.412 | 43 | 19 |

$t$ is the annealing time in hours and $T$ (°C) is the annealing temperature. $L$ is the arithmetic MTL. S.E. is the standard error of the mean. S.D. is the standard deviation of the sample. $N$ is the number of tracks measured and $A$ (°) is the arithmetic mean angle of tracks to the $c$-axis.
All samples etched in 5 M $HNO_3$ for 20 s at 20 ± 1 °C. Only TINTs measured. Data in italics have been acquired by using $^{252}Cf$ fission fragment irradiation (see Barbarand et al., 2003). $L = 0$ means no tracks can be seen in the sample; "track density too low" indicates that tracks can be seen but no MTL could be measured.

Table 12
Fission-track annealing data measured for apatite UMB

| $t$ (h) | $T$ (°C) | Analyst #1 | | | | | | | Analyst #2 | | | | | | | Analyst #3 | | | | | | |
|---|---|---|---|---|---|---|---|---|---|---|---|---|---|---|---|---|---|---|---|---|---|---|
| | | $L$ (μm) | ± S.E. | ± S.D. | $N$ | $L/L_0$ | $A$ (°) | ± S.D. | $L$ (μm) | ± S.E. | ± S.D. | $N$ | $L/L_0$ | $A$ (°) | ± S.D. | $L$ (μm) | ± S.E. | ± S.D. | $N$ | $L/L_0$ | $A$ (°) | ± S.D. |
| 0 | | 15.86 | 0.12 | 0.76 | 41 | 1 | 58 | 21 | 16.20 | 0.11 | 0.94 | 80 | 1 | 57 | 16 | 15.75 | 0.12 | 0.62 | 29 | 1 | 58 | 22 |
| 10 | 200 | 14.85 | 0.08 | 0.75 | 100 | 0.936 | 61 | 21 | | | | | | | | 14.96 | 0.08 | 0.76 | 103 | 0.950 | 55 | 22 |
| 10 | 240 | 14.19 | 0.07 | 0.71 | 100 | 0.895 | 57 | 20 | 14.09 | 0.09 | 0.91 | 103 | 0.870 | 62 | 20 | 14.20 | 0.06 | 0.61 | 101 | 0.902 | 64 | 17 |
| 10 | 275 | 13.11 | 0.10 | 1.03 | 101 | 0.827 | 58 | 20 | 13.12 | 0.08 | 0.83 | 101 | 0.810 | 60 | 18 | 13.19 | 0.09 | 0.88 | 102 | 0.837 | 56 | 18 |
| 10 | 280 | 13.18 | 0.10 | 1.01 | 100 | 0.831 | 54 | 20 | 13.08 | 0.09 | 0.90 | 103 | 0.807 | 57 | 20 | 13.11 | 0.09 | 0.87 | 100 | 0.832 | 54 | 20 |
| 10 | 300 | 11.59 | 0.13 | 1.15 | 82 | 0.731 | 60 | 21 | 11.61 | 0.12 | 1.02 | 73 | 0.717 | 61 | 18 | 11.70 | 0.11 | 0.92 | 69 | 0.743 | 57 | 20 |
| 10 | 312 | 10.09 | 0.14 | 1.39 | 101 | 0.636 | 61 | 21 | | | | | | | | 10.39 | 0.09 | 0.94 | 100 | 0.660 | 55 | 21 |
| 10 | 320 | 9.92 | 0.18 | 1.60 | 80 | 0.625 | 50 | 24 | | | | | | | | 10.09 | 0.16 | 1.52 | 93 | 0.641 | 44 | 23 |
| 10 | 325 | 8.70 | 0.21 | 2.14 | 100 | 0.549 | 49 | 18 | 8.61 | 0.19 | 1.86 | 101 | 0.531 | 50 | 20 | 8.57 | 0.17 | 2.36 | 200 | 0.544 | 49 | 21 |
| 10 | 335 | track density near zero | | | | | | | track density near zero | | | | | | | track density near zero | | | | | | |
| 100 | 210 | 14.35 | 0.09 | 0.90 | 100 | 0.905 | 59 | 22 | | | | | | | | 14.43 | 0.09 | 0.88 | 102 | 0.916 | 58 | 20 |
| 100 | 255 | 13.08 | 0.09 | 0.85 | 100 | 0.825 | 54 | 21 | | | | | | | | 13.17 | 0.09 | 0.76 | 72 | 0.836 | 58 | 19 |
| 100 | 275 | 11.68 | 0.10 | 0.96 | 100 | 0.736 | 58 | 21 | | | | | | | | 11.50 | 0.09 | 0.87 | 101 | 0.730 | 61 | 19 |
| 100 | 287 | 10.17 | 0.13 | 1.25 | 100 | 0.641 | 61 | 23 | | | | | | | | 10.33 | 0.10 | 1.03 | 101 | 0.656 | 57 | 20 |
| 100 | 295 | 8.09 | 0.33 | 2.79 | 71 | 0.510 | 48 | 20 | | | | | | | | 6.55 | 0.35 | 3.03 | 74 | 0.416 | 54 | 21 |
| 1000 | 185 | | | | | | | | | | | | | | | 14.63 | 0.09 | 0.81 | 91 | 0.929 | 56 | 20 |
| 1000 | 225 | 13.40 | 0.13 | 0.89 | 44 | 0.845 | 62 | 19 | | | | | | | | 13.25 | 0.16 | 0.84 | 30 | 0.841 | 57 | 18 |
| 1000 | 250 | 11.69 | 0.10 | 0.92 | 82 | 0.737 | 58 | 21 | | | | | | | | 11.46 | 0.09 | 0.92 | 100 | 0.728 | 58 | 21 |
| 1000 | 266 | 10.33 | 0.12 | 1.19 | 100 | 0.651 | 51 | 21 | | | | | | | | 9.65 | 0.18 | 1.77 | 100 | 0.613 | 50 | 22 |

$t$ is the annealing time in hours and $T$ (°C) is the annealing temperature. $L$ is the arithmetic MTL. S.E. is the standard error of the mean. S.D. is the standard deviation of the sample. $N$ is the number of tracks measured and $A$ (°) is the arithmetic mean angle of tracks to the $c$-axis.
All samples etched in 5 M $HNO_3$ for 20 s at 20 ± 1 °C. Only TINTs measured. Data in italics have been acquired by using $^{252}Cf$ fission fragment irradiation (see Barbarand et al., 2003). $L = 0$ means no tracks can be seen in the sample; "track density too low" indicates that tracks can be seen but no MTL could be measured.

Table 13
Fission-track annealing data measured for apatite UNK

| $t$ (h) | $T$ (°C) | Analyst #1 | | | | | | | Analyst #2 | | | | | | | Analyst #3 | | | | | | |
|---|---|---|---|---|---|---|---|---|---|---|---|---|---|---|---|---|---|---|---|---|---|---|
| | | $L$ (μm) | ± S.E. | ± S.D. | $N$ | $L/L_0$ | $A$ (°) | ± S.D. | $L$ (μm) | ± S.E. | ± S.D. | $N$ | $L/L_0$ | $A$ (°) | ± S.D. | $L$ (μm) | ± S.E. | ± S.D. | $N$ | $L/L_0$ | $A$ (°) | ± S.D. |
| 0 | | 15.69 | 0.09 | 0.88 | 100 | 1 | 57 | 22 | 15.94 | 0.11 | 0.96 | 76 | 1 | 56 | 21 | 15.63 | 0.13 | 0.89 | 49 | 1 | 53 | 24 |
| 10 | 200 | 14.74 | 0.07 | 0.74 | 100 | 0.939 | 57 | 20 | | | | | | | | 14.61 | 0.08 | 0.83 | 102 | 0.935 | 58 | 17 |
| 10 | 240 | 13.48 | 0.08 | 0.78 | 100 | 0.859 | 57 | 23 | 13.60 | 0.09 | 0.74 | 75 | 0.853 | 51 | 23 | 13.25 | 0.13 | 0.87 | 45 | 0.848 | 60 | 19 |
| 10 | 275 | 11.96 | 0.09 | 0.90 | 100 | 0.762 | 57 | 17 | 12.23 | 0.07 | 0.74 | 101 | 0.767 | 57 | 20 | 11.88 | 0.11 | 1.08 | 94 | 0.760 | 56 | 18 |
| 10 | 280 | 11.34 | 0.10 | 1.02 | 100 | 0.723 | 60 | 20 | 11.79 | 0.08 | 0.83 | 102 | 0.740 | 59 | 17 | 11.34 | 0.09 | 0.91 | 94 | 0.726 | 54 | 17 |
| 10 | 300 | *9.17* | *0.23* | *2.14* | *88* | *0.584* | *52* | *23* | *9.22* | *0.20* | *1.91* | *89* | *0.578* | *49* | *19* | *8.25* | *0.28* | *2.82* | *101* | *0.528* | *54* | *21* |
| 10 | 312 | *6.17* | *0.30* | *3.03* | *100* | *0.393* | *38* | *22* | | | | | | | | *4.30* | *0.33* | *2.93* | *80* | *0.275* | *51* | *21* |
| 10 | 320 | *track density near zero* | | | | | | | *track density near zero* | | | | | | | *4.81* | *0.77* | *2.44* | *11* | *0.308* | | |
| 10 | 325 | *track density near zero* | | | | | | | *track density near zero* | | | | | | | *3.23* | *0.35* | *1.31* | *14* | *0.207* | | |
| 10 | 335 | 0 | | | | | | | | | | | | | | 0 | | | | | | |
| 100 | 210 | 14.13 | 0.09 | 0.87 | 100 | 0.901 | 59 | 19 | | | | | | | | 13.93 | 0.10 | 0.89 | 86 | 0.891 | 57 | 19 |
| 100 | 255 | 11.04 | 0.11 | 0.87 | 64 | 0.704 | 59 | 19 | | | | | | | | 10.94 | 0.11 | 1.15 | 102 | 0.700 | 60 | 18 |
| 100 | 275 | *9.87* | *0.14* | *1.35* | *100* | *0.629* | *41* | *18* | | | | | | | | *7.55* | *0.29* | *2.88* | *101* | *0.483* | *52* | *18* |
| 100 | 287 | *6.82* | *1.80* | *2.55* | *3* | *0.435* | | | | | | | | | | *4.42* | *0.46* | *2.90* | *40* | *0.283* | *43* | *22* |
| 100 | 295 | track density near zero | | | | | | | | | | | | | | track density near zero | | | | | | |
| 1000 | 185 | 13.81 | 0.08 | 0.84 | 100 | 0.880 | 61 | 17 | | | | | | | | 13.99 | 0.07 | 0.74 | 100 | 0.895 | 60 | 17 |
| 1000 | 225 | 12.14 | 0.08 | 0.82 | 100 | 0.774 | 62 | 19 | | | | | | | | 12.05 | 0.09 | 0.87 | 102 | 0.771 | 55 | 19 |
| 1000 | 250 | 9.39 | 0.24 | 1.20 | 24 | 0.598 | 50 | 16 | | | | | | | | 8.15 | 0.33 | 2.51 | 59 | 0.521 | 51 | 19 |
| 1000 | 266 | 0 | | | | | | | | | | | | | | 0 | | | | | | |

$t$ is the annealing time in hours and $T$ (°C) is the annealing temperature. $L$ is the arithmetic MTL. S.E. is the standard error of the mean. S.D. is the standard deviation of the sample. $N$ is the number of tracks measured and $A$ (°) is the arithmetic mean angle of tracks to the $c$-axis.
All samples etched in 5 M $HNO_3$ for 20 s at 20 ± 1 °C. Only TINTs measured. Data in italics have been acquired by using $^{252}Cf$ fission fragment irradiation (see Barbarand et al., 2003). $L = 0$ means no tracks can be seen in the sample; "track density too low" indicates that tracks can be seen but no MTL could be measured.

Table 14
Fission-track annealing data measured for apatite WIL

| $t$ (h) | $T$ (°C) | Analyst #1 | | | | | | | Analyst #2 | | | | | | | Analyst #3 | | | | | | |
|---|---|---|---|---|---|---|---|---|---|---|---|---|---|---|---|---|---|---|---|---|---|---|
| | | $L$ (μm) | ± S.E. | ± S.D. | $N$ | $L/L_0$ | $A$ (°) | ± S.D. | $L$ (μm) | ± S.E. | ± S.D. | $N$ | $L/L_0$ | $A$ (°) | ± S.D. | $L$ (μm) | ± S.E. | ± S.D. | $N$ | $L/L_0$ | $A$ (°) | ± S.D. |
| 0 | | 15.74 | 0.07 | 0.71 | 100 | 1 | 58 | 16 | 16.04 | 0.08 | 0.86 | 110 | 1 | 61 | 18 | 15.89 | 0.08 | 0.78 | 101 | 1 | 58 | 13 |
| 10 | 200 | 14.63 | 0.09 | 0.90 | 100 | 0.929 | 57 | 18 | | | | | | | | 14.75 | 0.07 | 0.70 | 101 | 0.928 | 62 | 14 |
| 10 | 240 | 13.34 | 0.08 | 0.75 | 100 | 0.848 | 61 | 16 | 13.36 | 0.08 | 0.87 | 107 | 0.833 | 56 | 17 | 13.51 | 0.08 | 0.78 | 102 | 0.850 | 61 | 15 |
| 10 | 275 | 12.17 | 0.09 | 0.85 | 100 | 0.773 | 58 | 22 | 12.18 | 0.08 | 0.83 | 102 | 0.759 | 54 | 19 | 12.23 | 0.08 | 0.78 | 107 | 0.770 | 52 | 19 |
| 10 | 280 | 11.67 | 0.09 | 0.90 | 100 | 0.741 | 61 | 18 | 11.70 | 0.08 | 0.82 | 105 | 0.729 | 58 | 18 | 11.66 | 0.08 | 0.81 | 102 | 0.734 | 57 | 14 |
| 10 | 300 | 9.33 | 0.22 | 2.18 | 100 | 0.593 | 54 | 19 | 9.48 | 0.14 | 1.40 | 100 | 0.591 | 56 | 18 | 9.35 | 0.21 | 2.10 | 101 | 0.588 | 54 | 19 |
| 10 | 310 | 9.76 | 0.16 | 1.63 | 101 | 0.620 | 53 | 21 | | | | | | | | 9.69 | 0.12 | 1.21 | 102 | 0.610 | 54 | 21 |
| 10 | 312 | *6.59* | *0.30* | *3.00* | *100* | *0.419* | *49* | *23* | *7.61* | *0.25* | *2.40* | *96* | *0.474* | *39* | *19* | *5.83* | *0.54* | *3.48* | *43* | *0.367* | *49* | *21* |
| 10 | 320 | 7.82 | 0.28 | 2.81 | 100 | 0.497 | 48 | 19 | 7.23 | 0.27 | 2.70 | 101 | 0.451 | 48 | 20 | 7.01 | 0.22 | 3.14 | 200 | 0.441 | 52 | 20 |
| 10 | 325 | *6.09* | *0.26* | *2.55* | *100* | *0.387* | *22* | *18* | | | | | | | | *4.12* | *0.26* | *2.55* | *100* | *0.259* | *46* | *21* |
| 10 | 335 | 0 | | | | | | | | | | | | | | 0 | | | | | | |
| 100 | 210 | 14.23 | 0.10 | 1.04 | 100 | 0.904 | 55 | 20 | | | | | | | | 14.10 | 0.07 | 0.71 | 101 | 0.887 | 60 | 17 |
| 100 | 255 | 12.03 | 0.10 | 0.97 | 100 | 0.764 | 55 | 24 | | | | | | | | 12.07 | 0.09 | 0.87 | 102 | 0.760 | 56 | 17 |
| 100 | 275 | 10.00 | 0.14 | 1.44 | 100 | 0.635 | 41 | 20 | | | | | | | | 8.53 | 0.24 | 2.44 | 102 | 0.537 | 51 | 19 |
| 100 | 287 | *8.39* | *0.21* | *2.08* | *100* | *0.533* | *30* | *17* | | | | | | | | *6.47* | *0.31* | *3.07* | *101* | *0.407* | *40* | *19* |
| 100 | 295 | track density near zero | | | | | | | track density near zero | | | | | | | track density near zero | | | | | | |
| 1000 | 185 | 13.93 | 0.08 | 0.79 | 100 | 0.885 | 60 | 15 | | | | | | | | 14.31 | 0.07 | 0.67 | 101 | 0.901 | 57 | 15 |
| 1000 | 225 | 12.20 | 0.09 | 0.88 | 100 | 0.775 | 58 | 15 | | | | | | | | 12.52 | 0.09 | 0.88 | 102 | 0.788 | 53 | 16 |
| 1000 | 250 | 9.90 | 0.14 | 1.39 | 100 | 0.629 | 52 | 19 | | | | | | | | 8.91 | 0.21 | 2.12 | 101 | 0.561 | 52 | 19 |
| 1000 | 266 | track density near zero | | | | | | | | | | | | | | track density near zero | | | | | | |
| 1000 | 275 | 0 | | | | | | | 0 | | | | | | | 0 | | | | | | |

$t$ is the annealing time in hours and $T$ (°C) is the annealing temperature. $L$ is the arithmetic MTL. S.E. is the standard error of the mean. S.D. is the standard deviation of the sample. $N$ is the number of tracks measured and $A$ (°) is the arithmetic mean angle of tracks to the $c$-axis.
All samples etched in 5 M $HNO_3$ for 20 s at 20 ± 1 °C. Only TINTs measured. Data in italics have been acquired by using $^{252}Cf$ fission fragment irradiation (see Barbarand et al., 2003). $L = 0$ means no tracks can be seen in the sample; "track density too low" indicates that tracks can be seen but no MTL could be measured.

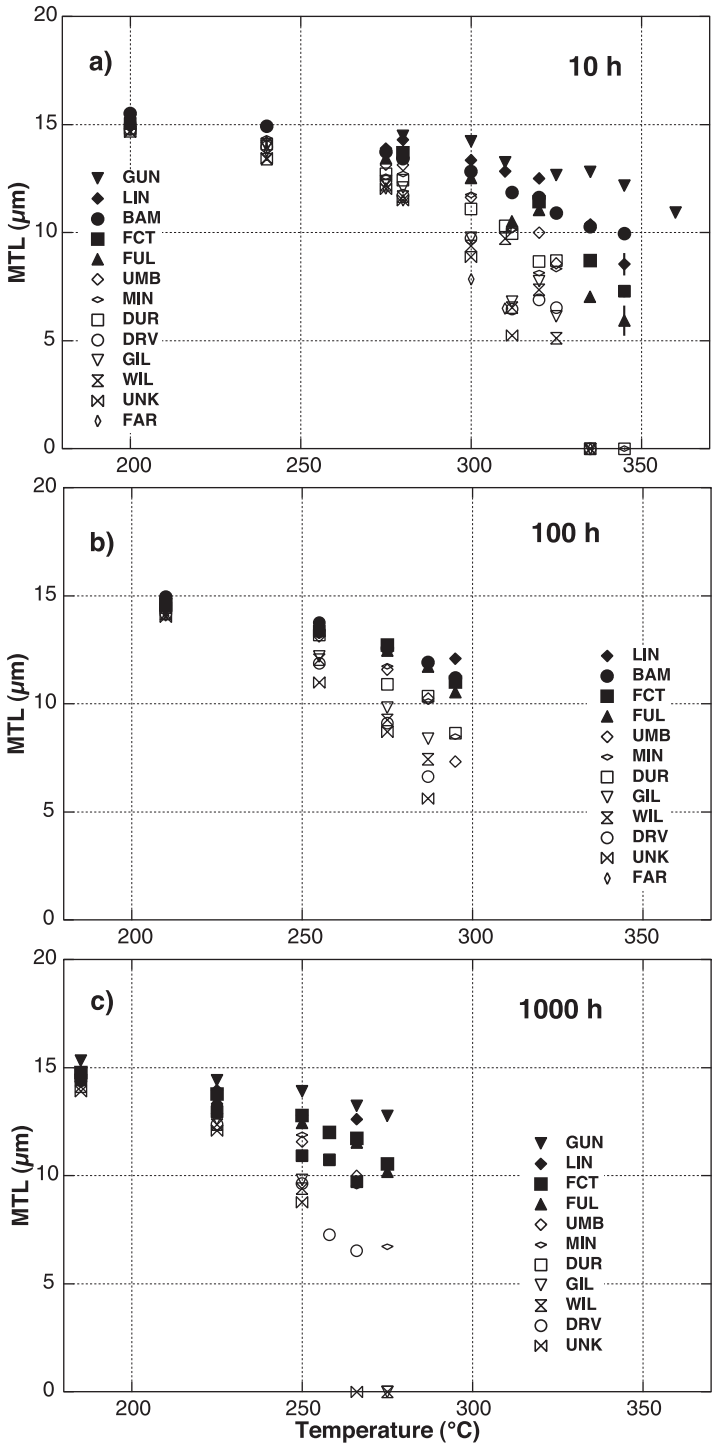


Fig. 2. Results of the FT annealing experiments: (a) 10, (b) 100 and (c) 1000 h. Open symbols represent samples with a Cl content $<0.1$ apfu ($\sim 0.35$ wt.%). Error at $\pm 1$ standard error is included in the size of the symbol.

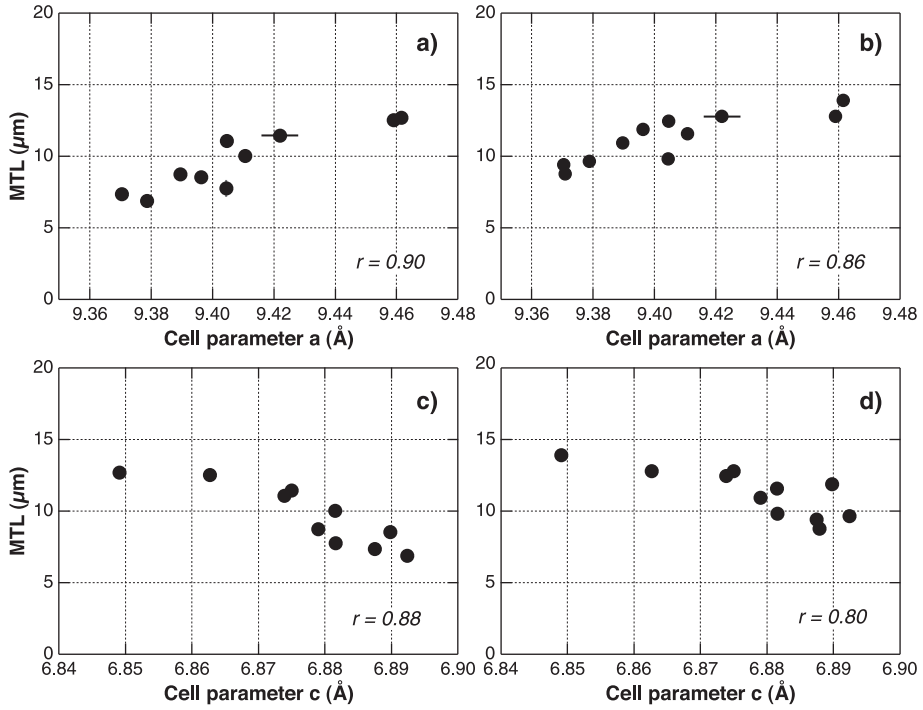


Fig. 3. Relationship between MTL and unit-cell parameters *a* and *c* for two representative annealing experiments: (a, c) 320 °C for 10 h and (b, d) 250 °C for 1000 h. Errors on *x* and *y* are ± 1 standard error and mainly lie within plotted points.

samples in 2 representative annealing experiments. These experiments have been selected because they cover the low MTL range where differences are greatest and are characterised by a high number of tracks measured for all samples. Similar relationships are observed for the other annealing experiments. The plots show a well-developed correlation between the level of annealing (as given by reduction in MTL) and unit-cell size, with $r>0.8$ in each case. Increasing MTL is associated with an increase in the cell parameter dimension *a* and with a decrease of the cell parameter dimension *c*. Cell parameter *a* shows a greater level of response to variation in MTL than unit *c* and thus represents a more sensitive parameter to use for monitoring compositional effects. Accordingly, parameter *a* is presented throughout this study although the conclusions drawn are equally valid for parameter *c*. The cell volume that combines these two parameters has not been used as it represents a mixture of the two cell parameter dimensions.

Carlson et al. (1999) have previously considered unit-cell dimensions, but did not explicitly report any systematic relationship between the unit cell and track annealing rate for a suite of apatites with a broader range of compositions than in our study. Using a subset of their data (omitting those apatites with less common compositions), the fit of their measured track lengths with the reported values of the unit-cell parameter *a* shows a broadly similar relationship to that presented in Fig. 3.

No systematic correlation is found between unit-cell parameters and MTL for the initial, unannealed samples because here MTL is controlled by the variable bulk-etching characteristics (Carlson et al., 1999; Barbarand et al., 2003).

The results in Fig. 3 show that the unit cell is a key indicator of an apatite's response to annealing. In the study of Carlson et al. (1999), unit-cell dimensions were considered, but it was concluded that a complex interplay between a range of different factors precluded any systematic relationship between the unit cell and track annealing rate. Our data indicate that for the samples studied here (which represent the range of compositions of most apatites derived from magmatic

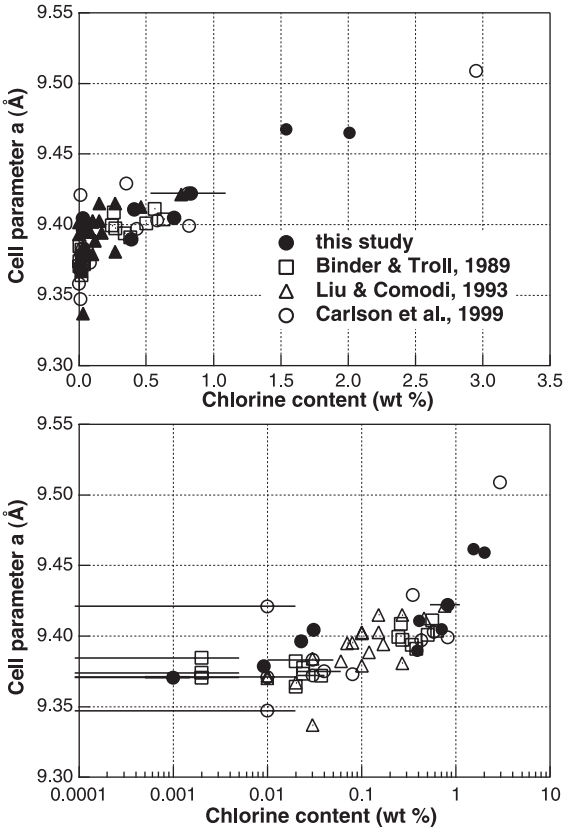


Fig. 4. Relationship between unit-cell parameter *a* and chlorine content using both linear and logarithmic X-scales. Chlorine content is expressed in weight percent to enable comparison with previously published data. Error bars ± 1 standard error and mainly lie within plotted points. Cell parameters from the four different data sets may be subject to systematic errors.

sources), this may not be the case. The dimensions of the unit cell are governed by bulk composition, although it is possible that most of the changes can be accounted for by relatively few elemental substitutions. In Section 5.2, we consider which elements exert the greatest influence on the apatite unit cell.

### 5.2. Controls on the unit-cell dimensions

#### 5.2.1. Chlorine

Substitution on the anion site has a major influence on apatite cell parameters. A large variation from 9.367 to 9.628 Å for parameter *a* is associated with the transition from F-apatite to Cl-apatite (Sudarsanan et al., 1972; Mackie et al., 1972). OH-apatite has a typical value of 9.424 Å. Variations of the parameter *c* are much less dispersed for F-apatite or OH-apatite at 6.884 and 6.879 Å, respectively (Sudarsanan et al., 1972; Sudarsanan and Young, 1969), to 6.764 Å for Cl-apatite (Mackie et al., 1972). Variation of the cell parameters thus can be explained in part by differing levels of chlorine substitution, as shown in Fig. 4, which combines the data of this study with published values.

For Cl contents above 0.1 apfu (~ 0.35 wt.%), the value of parameter *a* shows a clear systematic

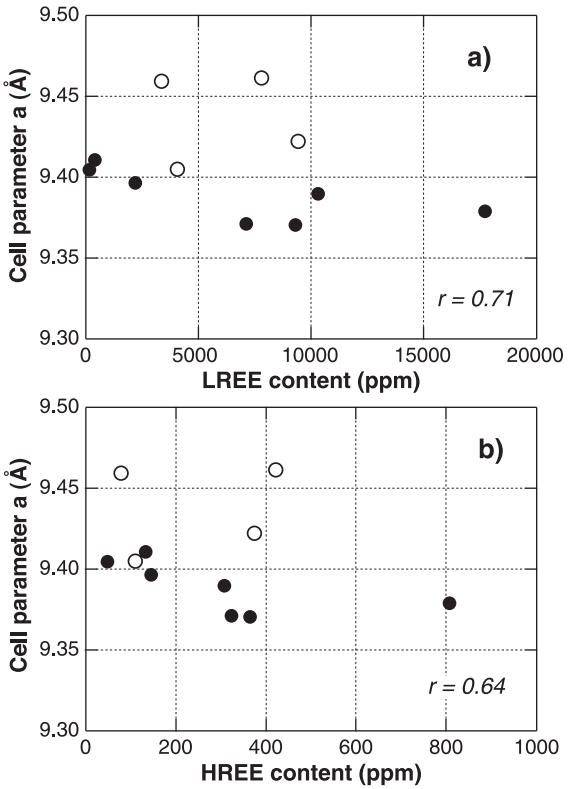


Fig. 5. Relationship between unit-cell parameter *a* and rare earth element content for (a) LREE and (b) HREE. Open symbols correspond to samples with Cl content >0.12 apfu (~ 0.40 wt.%) where chlorine exerts the major control on cell parameters. Samples with Cl >0.12 apfu are represented but not considered for the correlation between cell parameters and REE contents. For samples with low content of chlorine (< 0.12 apfu), cell parameter *a* value is associated with the content of rare earth elements: samples with the lowest REE substitution have a larger cell parameter *a* than samples with high levels of REE substitution. Error on the cell parameter is included in the size of the symbol. Correlation coefficients calculated only for the low-chlorine samples represented by solid points.

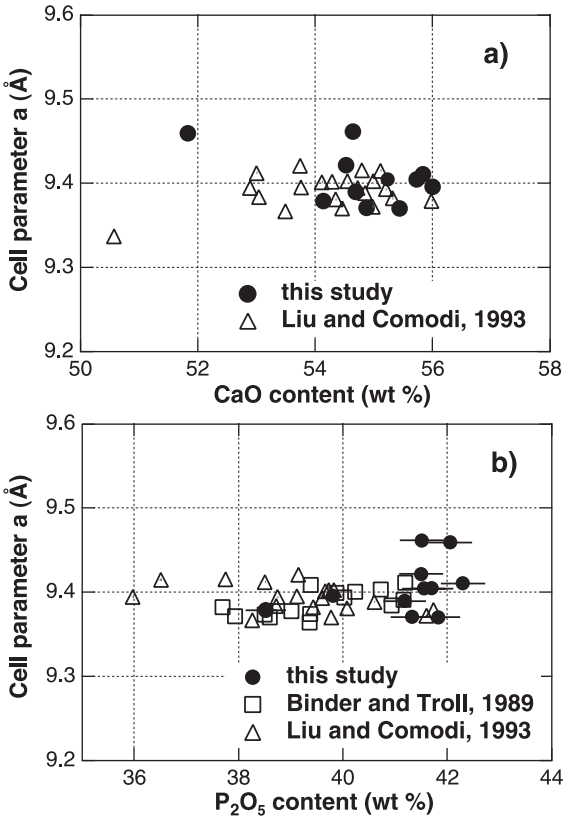


Fig. 6. Relationships between unit-cell parameter *a* and principal compositional components of apatite. (a) CaO and (b) $P_2O_5$. Errors are ± 1 standard error and lie mainly within the plotted points.

increases (Fig. 4). The control of the hydroxyl ion is small, but a slight increase of OH is paralleled by a slight increase in parameter *a*. The more OH-rich apatite, GIL (OH = 1.45 apfu, 1.30 wt.%) is characterised by a value for parameter *a* very close to that of sample DUR with no hydroxyl component (9.4045–9.3896 Å, respectively).

### 5.2.2. Rare earth elements

Rare earth elements cause variation in unit-cell size because of the difference of ionic radius and balancing charge mechanism associated with their substitution in the Ca site (Fleet and Pan, 1997). La and Ce have larger radii than Ca, while Nd to Lu have smaller radii (lanthanide contraction) than Ca, irrespective of the site of substitution and co-ordination number. Preferential substitution in apatite is predominately light REE replacement in the Ca(II) site (Fleet and Pan, 1995), with typical concentrations of < 0.5 oxide wt.% for the light REE, La, Ce, Pr and Nd, and < 100 ppm for other REE. Substitution of light REE in natural apatite results in an increase in size of the structure as their ionic radii are larger than the Ca radius (Hughes et al., 1991b). Fleet and Pan (1995) reported that the unit-cell volume for single REE-substituted fluorapatite generally decreased monotonically through the 4f transition-metal series, implying that structural change in response to spatial accommodation of REE also varied monotonically. The change in the crystal structure associated with increasing amounts of REE has so far not been investigated in detail.

The results presented in this study show some correlation between the REE concentration and the variation in cell parameters if samples with Cl content >0.12 apfu (~ 0.40 wt.%) are not considered (Fig. 5).

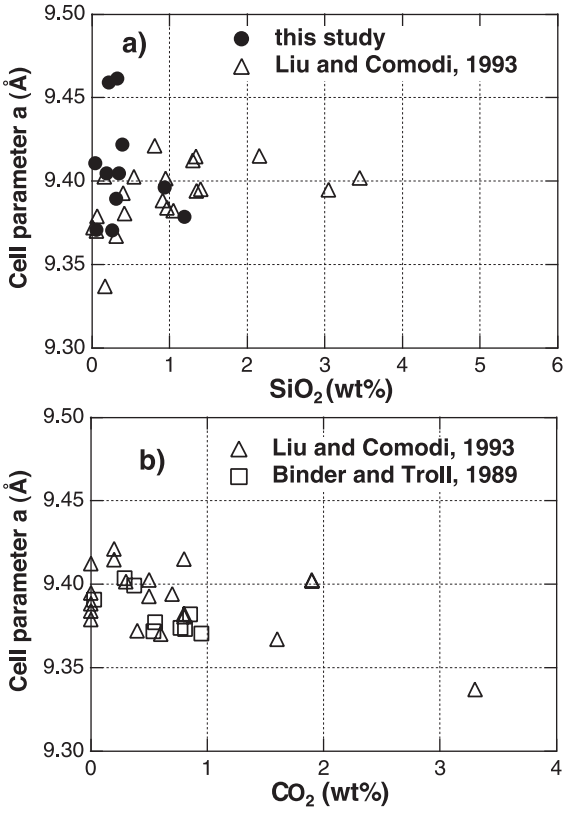


Fig. 7. Relationship between cell parameter *a* and minor substituted components (a) $SiO_2$ and (b) $CO_2$. Only apatites with Cl < 0.1 apfu (~ 0.35 wt.%) are shown. Errors are ± 1 standard error and are within plotted points.

The increased substitution correlation with variation of the unit cell, which can be assumed to mirror the REE substitution as the coupled substitution REE + Na, occurs to maintain the charge balance (Rønsbo, 1989).

*5.2.3. Other substitutions*

Our study confirms previous findings (Binder and Troll, 1989; Liu and Comodi, 1993) that there is no apparent correlation of apatite unit-cell parameter *a* with the abundances of the main components Ca and P (Fig. 6). $SiO_2$ and $CO_3$ substituted into the P site to balance the introduction of monovalent and trivalent cations into the Ca site have been reported to control the cell parameters (Liu and Comodi, 1993). However, results from this study for $SiO_2$ plotted with those from Binder and Troll (1989) and Liu and Comodi (1993) suggest no apparent correlation (Fig. 7). Those samples with chlorine contents >0.1 apfu show marginally greater values for cell parameter *a*, most probably reflecting the direct influence of chlorine. As $CO_3$ is only found in significant concentrations in carbonatites and mantle rocks, it can be dismissed in discussion of common apatite crystals of magmatic origin.

Other elements (Fe, Mn, Sr), present usually as minor substitutions in apatites, may introduce slight changes to the unit-cell parameters. Ionic radii of 0.96 for Mn and 1.21 for Sr in co-ordination IX and VII do not match the Ca radii (Shannon, 1976; Hughes et al., 1991b). This study suggests that Sr, which is substituted on the Ca(II) site, is the only element to show a clear relationship with parameter *a*. However, the samples used in this study have comparatively low concentrations of Fe, Mn and Sr, and further investigation into these substitutions is required. Carlson et al. (1999) found that two F-apatites characterised by out-of-range values of

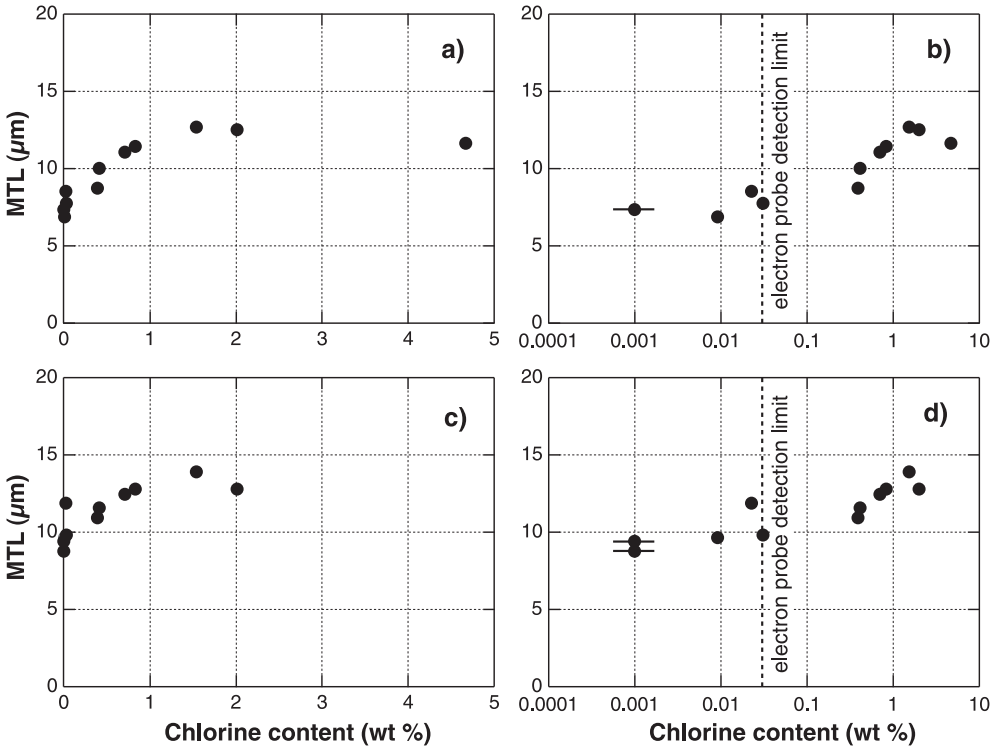


Fig. 8. Relationship between mean track length and chlorine content for two representative annealing experiments: (a, b) 320 °C for 10 h and (c, d) 250 °C for 1000 h. Data are presented using linear (a, c) and logarithmic X-scale (b, d). Errors are ± 1 standard error and are mainly within plotted points. (b) and (d) show that MTL variations still exist for concentrations below the EPMA chlorine detection limit (0.1 apfu or 0.03 wt.%; Seifert et al., 2000).

parameter *a* of 9.347 and 9.421 Å showed anomalous annealing properties relative to Durango and were enriched in Mn (7.04 oxide wt.%) and Sr (9.15 oxide wt.%), respectively.

Thus, consideration of REE substitution suggests that it may exert an important control on FT annealing as it requires other elements (Na, Si, C) to be introduced into the lattice to maintain charge balance. This REE substitution and the associated Na, Si and C substitutions change the unit-cell parameters.

### 5.3. So what controls apatite fission-track annealing?

This study has shown that variation in FT annealing is correlated with the apatite cell parameters and thus is linked to crystallographic structure, which, in turn, is controlled by apatite composition. We have considered above the principal elemental controls on apatite structure and have found that no single substitution can explain the bulk change in lattice parameters, although for concentrations >0.25 apfu (~ 0.85 wt.%) chlorine appears to dominate. For the more F-rich apatites (Cl < ~ 0.1 apfu, 0.4 wt.%), the most common in nature (e.g. Bergman and Corrigan, 1996; Table 4 in Carlson et al., 1999), substitutions such as LREE exert a significant influence on unit-cell parameters and hence on annealing.

Fig. 8 shows plots of chlorine content vs. MTL for two representative annealing experiments (320 °C for 10 h and 250 °C for 1000 h). The trend of increasing MTL with greater chlorine content is clear, although in each case the longest length does not correspond to the greatest Cl-content (also reported by Carlson et al., 1999), possibly a consequence of less precise measurement due to the larger etch pits or the affect of another substitution. Significant variation in MTL is also recorded in the low to zero Cl apatites (< 0.1 apfu), with values ranging from $6.88 \pm 0.25$ to $8.54 \pm 0.26$ μm (320 °C for 10 h; $\pm 1$ S.E.M.) and $8.77 \pm 0.33$ to $11.88 \pm 0.10$ μm (250 °C for 1000 h). Linear scale plotting of Cl-content (Fig. 8a and c) disguises small differences in Cl content. In Fig. 8b and d, the data are replotted using a log scale for Cl content with spectrophotometry being used for those samples whose chlorine content lie below EPMA detection limit. A poorly defined relationship exists between MTL and Cl content indicating that, for fluorapatites at least, other elemental substitutions make a significant contribution to the measured responses in FT annealing.

Fig. 9 shows MTL vs. Ce content in ppm for two representative annealing steps. Ce has been selected as it represents the rare earth element most frequently substituted in the apatite structure (Fleet and Pan, 1995). Similar relationships are found for the other LREE, especially when Ce and La are present in high amounts. For fluorapatites with Cl < 0.1 apfu, MTL shows an inverse correlation with Ce content, suggesting that annealing rate increases with greater levels of Ce substitution. Apatite MIN has the greatest

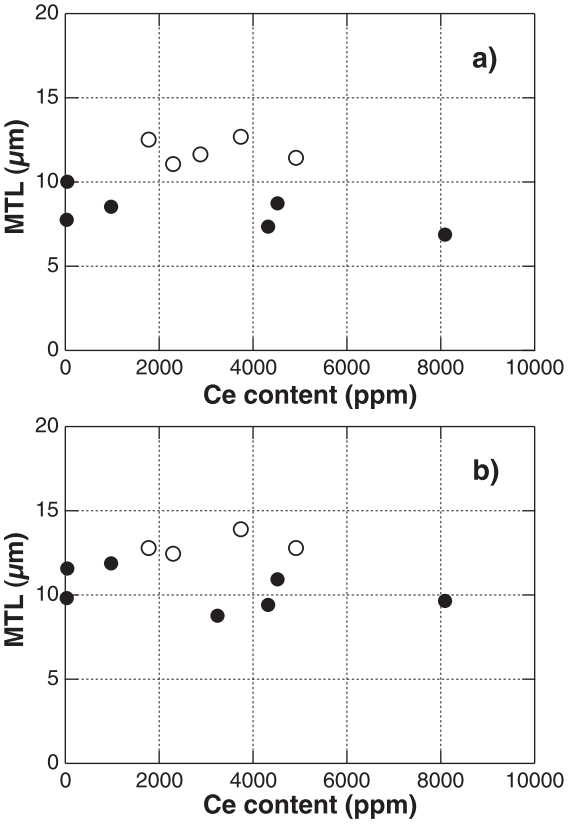


Fig. 9. Relationship between mean track length and Ce content for two representative annealing experiments: (a) 320 °C for 10 h and (b) 250 °C for 1000 h. Ce content is used to monitor the REE variations: because of the preferential substitution of light REE, Ce represents the element commonly present in the greatest abundance in the studied samples. Open symbols represent chlorapatite (Cl >0.12 apfu, ~ 0.4 wt.%) where the main control on the FT annealing is the chlorine content. For fluorapatite (Cl < 0.12 apfu), light REE also represents a major control. Errors at $\pm 1$ standard error lie within the plotted points.

resistance to annealing among these fluorapatites and is also characterised by the lowest REE content. As discussed above, for samples with Cl>0.1 apfu, Cl is the dominant control on track annealing, effectively masking any effect from Ce or other REE substitutions.

The presence of large numbers of cations substituted for Ca exhibits some correlation with the annealing properties of F-apatites (Crowley et al., 1991; Carlson et al., 1999). In our study, little information about how Sr, Mn and Fe control mean track length was forthcoming because of the low concentrations of the elements in our samples (see Table 1). Seemingly very high concentrations are required to modify apatite track annealing properties; in the studies cited above, samples with 4.44 wt.% of SrO (Crowley et al., 1991), 7.04 wt.% of Mn and 9.15 wt.% of SrO (Carlson et al., 1999) were considered. For most apatites where Sr, Mn and Fe concentrations are low, the effect of these elements may be safely ignored.

## 6. How can controls of FT annealing best be monitored?

Reconstruction of thermal history from the FT parameters measured for a sample is the prime objective of most FT analyses. Since compositional variation exerts a substantial influence on the rate of fission-track annealing in apatite, the determination of the composition of an apatite sample is a vital prerequisite. However, thermal history modelling is based on annealing algorithms established for reference apatites of specific compositions. The similarity or difference between the compositions of sample and reference apatites will determine the degree of applicability of a modelling program to an individual sample. This implies the necessity to determine bulk composition for every apatite grain analysed, a proposition neither practical nor possible because several destructive analytical techniques are required to describe fully and adequately an apatite's composition.

Attempts to consider bulk chemistry have been already proposed through the use of ionic porosity (Carlson et al., 1999). Ionic porosity is a property of the material structure and represents the volume of the cell not occupied by the cations plus the anions (Fortier and Giletti, 1989). It has been reported as explaining the variation of retentivity of fission tracks and the kinetics of Pb loss in U-bearing minerals (Carlson, 1990; Dahl, 1997). However, determination of ionic porosity requires unit-cell volume data and is, therefore, also not a practical possibility for single-grain analysis.

Two procedural approaches have been used to circumvent this apparent impasse. Firstly, measurement can be made of the abundances of only those elements whose affect on annealing is greatest. Secondly, apatites can be excluded from consideration if their compositions differ by more than a defined amount from the composition of apatite in the calibrating annealing experiments.

Recognition of the major role played by chlorine in track annealing, and its ready measurement by EPMA at abundances above ~ 0.03 wt.% has prompted some analysts to determine chlorine exclusively. This represents a pragmatic response and has, in principle, the benefit of being able to relate a sample and its FT data to a variable annealing model defined by the F/Cl anion ratio. Arguably, this is better than assuming that an annealing model constructed for an apatite of a single composition is equally applicable to each apatite grain in every sample, irrespective of composition: e.g. accepting that the Laslett et al.'s (1987) annealing model based on Durango data is universally applicable. However, a chlorine-only approach fails to take into account changes in lattice parameters and annealing when fluorapatite samples are considered or when apatite varieties containing unusual cation and anion substitutions (e.g. Sr, Mn, Fe, REE and Si) are encountered. Fission-track annealing response for samples with low chlorine, high REE or exotic cation content cannot be investigated by the measurement of chlorine alone. Although exotic elemental exchanges (e.g. high concentrations of Sr, Mn and Fe) are rare, most apatites in the geological environment are low in chlorine. The measurement of only chlorine to account for variation in fission-track annealing is thus an oversimplification.

Ideally, an alternative approach is needed to assess the response of an apatite grain to annealing. Structure, as given by unit-cell parameters, represents the summed affect of substitutions in the apatite lattice and, as demonstrated in this study, shows good

correlation with degree of annealing as measured by MTL (see Fig. 3). While omitting the detailed interplay of individual substitutions by measuring the overall resultant apatite structure is both attractive and elegant, the reality is that application of X-ray diffractometry on a grain-by-grain basis after etching, irradiation and counting of fission tracks is equally impractical.

Fourier transform infra-red microspectroscopy has been shown as a possible non-destructive tool for assessment of apatite composition, but again the method provides a measure of only the F/Cl ratio, and precision is not well defined (Siddall and Hurford, 1998).

An alternative approach is to use apatite solubility as an integrated measure of bulk composition: the size and shape of the well-defined etch pit outcropping on the viewed surface varies according to the apatite composition. Donelick (1993) demonstrated a correlation between track etch-pit size and Cl content, while Burtner et al. (1994) considered that each of these parameters might be used independently of the other as a stand-alone indicator of kinetic response. In practice, measurements are made along the two-dimensional cross-sections of etch pits, $D_{par}$ being the pit length parallel to the *c*-crystallographic axis, $D_{per}$ the pit width perpendicular to the *c*-axis (Burtner et al., 1994). The aspect ratio of the etch pit perhaps provides the most useful measure of discrimination. The method has not been widely adopted, most probably because of the small size of the pits (in particular measurement of the smaller $D_{per}$) and apparently imprecise measurement using an optical microscope and digitising tablet. Burtner et al. (1994) proposed measurement of between one and five etch figures per sample for natural fission tracks. However, a potential advantage of the technique is that the sample size may be large as every pit (i.e. each outcropping sub-surface track) in an apatite grain can be measured.

Table 1 includes *c*-parallel etch-pit lengths ($D_{par}$) for unannealed aliquots of each sample in this study,

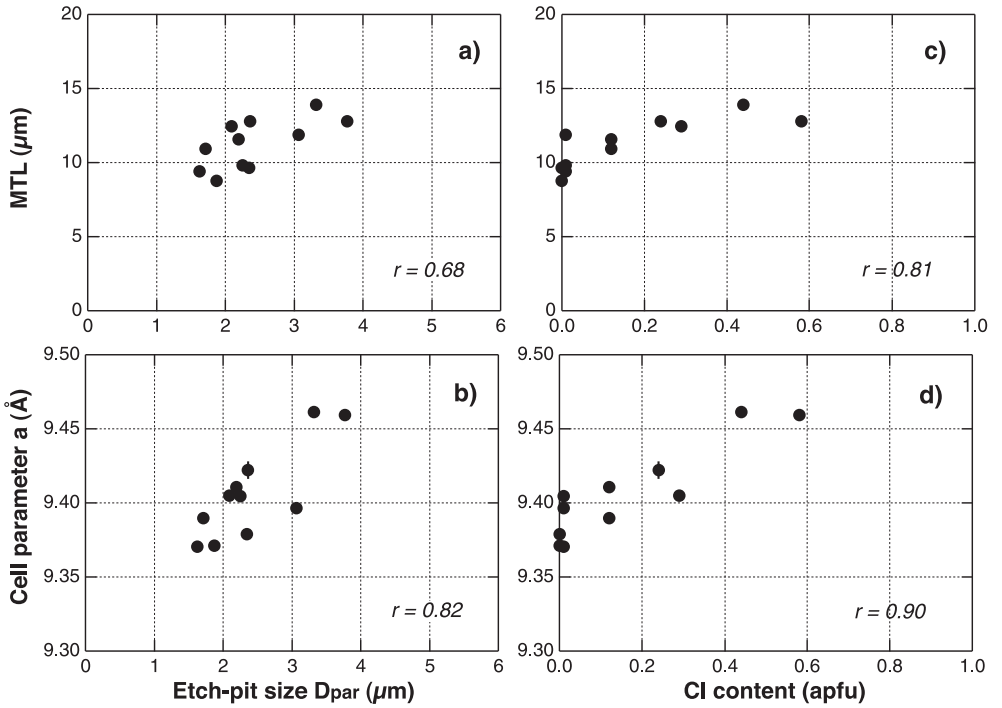


Fig. 10. Relationship between the mean track length and cell parameter *a* vs. etch-pit size (plots b and d) and chlorine content (plots a and c) for a single representative annealing experiment at 250 °C for 100 h. In addition, etch-pits values have been measured on unannealed sections for each sample.

with values ranging between 1.62 ± 0.03 and 5.22 ± 0.04 μm (± 1 standard error). Increase in pit size generally, but not absolutely, equates with increase in chlorine content. No systematic differences were found between etch-pit sizes in annealed and unannealed samples, pit size appearing to be a function solely of apatite solubility. Fig. 10 shows etch-pit size ($D_{par}$) and chlorine content plotted against the unit-cell parameter *a* and MTL measured for one representative annealing experiment at 250 °C for 100 h. The increase in etch-pit size is mirrored by increases in both MTL (Fig. 10a) and cell parameter *a* (Fig. 10b) with modest levels of correlation, apatite solubility including the net affect of *all* substitutions. Thus, etch-pit size appears a good measure of relative unit-cell size and, accordingly, a feasible means of assessing annealing rate of an individual apatite grain. Some residual scatter is present in the dataset: sample BAM with the largest etch-pit size was excluded because it relates to a rare monoclinic form of apatite. In this study, where the induced track density is high, 100 etch pits were measured for each sample. This approach has the clear advantage of simplicity and ease of measurement. Even though etch-pit size is determined at least in part by composition, the approach does not require absolute evaluation of composition for it to function as useful measurement system. However, as with any attempt to correlate composition and annealing, robust use of etch-pit data requires a variable annealing model calibrated against the response of samples with differing etch-pit sizes.

## 7. Conclusions

This study underlines the important control that apatite composition has on the rate of fission-track annealing and hence on the prediction of thermal history for a field sample. This control represents the summed effects of the type and amount of elemental substitution together with the substitution sites. These factors govern the unit-cell parameters, which represent an integrated measure of apatite composition.

In samples measured in this study, for any given period and temperature of heating, the degree of FT annealing shows a well-developed correlation with composition as represented by the unit-cell parameters: increase in MTL correlates directly with cell parameter *a* and inversely with parameter *c*. This differs somewhat from the data of Carlson et al. (1999) who, working with a broader range of apatite compositions, found poorer correlation of unit-cell parameter and composition. We found no correlation between unit-cell parameters and MTL in unannealed samples where track length is controlled by apatite solubility.

As reported previously, chlorine substitution exerts a major influence on annealing, with Cl-rich apatites being more resistant to annealing. Increased chlorine substitution is reflected by an increase in cell parameter *a* and decrease in parameter *c*.

For fluorapatites where Cl < 0.03 apfu (< ~ 0.1 wt.%) and even below the detection limits of EPMA (0.1 apfu, 0.03 wt.%), significant variation in MTL is still found, but this does not correlate well with chlorine amounts determined by spectrophotometry, implying other elemental substitutions are responsible for different FT annealing responses. Rare earth elements exhibit a modest correlation with cell parameter *a* and also with the level of FT annealing: for a suite of apatites annealed under similar conditions, MTL decreases with increasing REE. Variation in abundances of Ca, P, $SiO_2$, Fe, Mn and Sr show that only Sr substituted on the Ca(II) site exhibits a clear influence on cell parameters. Low strontium contents found in most apatites suggests that, for routine sample analysis, the influence of Sr on FT annealing may be limited, although this merits further investigation.

Since annealing appears to vary with composition, the use of an annealing algorithm and predictive model based on apatite of a single composition to interpret all sample data represents an approximation. Determination of bulk composition of each apatite in every sample is impractical, requiring multiple, often destructive analytical techniques. XRD measurement of unit-cell apatite-by-apatite, while attractive, is similarly impractical as a routine tool.

Pragmatically, two alternative, perhaps complementary approaches (each previously described), can be used to improve interpretation of sample data.

Firstly, EPMA can rapidly determine chlorine content, which certainly represents the major compositional influence on FT annealing. However, fluorapatites comprise the majority of apatites from upper

crustal samples and, despite having low Cl contents, variation in MTL still exists. REE exert a significant influence on FT annealing for such chlorine-poor apatites, ideally requiring analysis by ICP-MS.

Secondly, apatite solubility reflects total composition and thus measurement of FT etch-pit size provides a clear correlation with cell parameter *a* and with MTL values determined for different apatites annealed under the same conditions. Our results support the proposal that etch-pit size is a valuable estimator of annealing rate of an individual apatite grain, albeit limited by the precision of measurement.

For practical determination of thermal history, each approach requires the determination and use of a variable annealing model calibrated against the FT annealing responses of samples with different chlorine contents and/or etch-pit sizes. Such consideration of the data reported here and published elsewhere will be presented in a later contribution.

## Acknowledgements

This study of FT annealing and composition in apatite has been generously supported by a research grant from Elf EP and by continuous encouragement from, and stimulating discussion with, Frédéric Walgenwitz from ElfF EP (Pau). JB has been supported by a Marie Curie fellowship of the European Community programme Energy, Environment and Sustainable Development under contract number ENK6-CT-1999-50002. ICP-MS analysis at the NERC ICP-MS facility, Kingston University was enabled through a grant ICP/179/1200 and we thank Kym Jarvis and Jo Greenwood (Centre for Earth and Environmental Science Research, Kingston University) for their assistance and forbearance. We are grateful to Jacques Morel (CRPG, Nancy, France) and Maurice Pagel (Université Paris-Sud, France) for generous help in experimental data acquisition, and to Paul Green and Ray Donelick for comment and constructive criticism of our thoughts and writings, even though we may not have heeded all their ideas. Rex Galbraith and Geoff Laslett assisted in planning the annealing experiments. Andy Gleadow and an anonymous referee offered helpful reviews of our paper. Assistance in locating and supplying various apatite crystals provided by Torgeir Garmo, Bill Kettley, Bart Kowallis, Rob Lavinsky, Gunnar Raade and Richard Tayler was a fundamental pre-requisite to this study and is gratefully acknowledged. **[PD]**

## Appendix A. Brief description of apatite samples

BAM: 15-mm brown crystal from Bamble, Telemark, Norway.
DRV: 50-mm green fluorapatite crystals from Ontario, Canada.
DUR: 20-mm gem-quality yellow apatite from Cerra de Mercado, Durango, Mexico (see Young et al., 1969).
FAR: Faraday, Ontario, Canada.
FCT: from a welded Fish Canyon Tuff in the San Juan Mountains of southern Colorado, USA (see Steven et al., 1967).
FUL: 20-mm lemon-coloured single crystal from Fulford, Eagle county, Colorado, USA.
GIL: 25-mm diameter tabular champagne-coloured crystal from Shigar mine, Khudayat, Skardu area, Gilgit, Pakistan.
GUN: crystals from altered volcanic ash beds GUN-F, middle Jurassic Carmel formation, southwest Utah, USA (see Kowallis et al., 1993).
LIN: part of a transparent gem-quality crystal from an unknown locality Linden.
MIN: 25-mm dark blue crystal from Capon Grosso, Minas Gerais, Brazil.
UMB: 30-mm lemon-coloured crystal from Umba, Tanzania.
UNK: 50-mm green-brown crystals from an unknown locality, possibly Canadian.
WIL: 20-mm lemon-green fluorapatite crystals from Liscombe deposits, Wilberforce, Ontario, Canada.

## References

Barbarand, J., Pagel, M., 2001a. Contrôle de la cinétique de cicatrisation des traces de fission dans les cristaux d'apatite: le rôle de la composition chimique. C. R. Acad. Sci. Paris 332, 259–265.

Barbarand, J., Pagel, M., 2001b. Cathodoluminescence study of apatite crystals. Am. Mineral. 86, 473–485.

Barbarand, J., Hurford, A.J., Carter, A., 2003. Variation in apatite

fission-track length measurement: implications for thermal history modelling. Chem. Geol. 198, 77–106 (this issue).

Ben Ghouma, N., 1995. Etude de l'influence de la composition de l'apatite sur la révélation et le recuit des traces de fission de l'uranium. Unpublished PhD thesis, Franche Comté University, Besançon, France, 257 pp.

Bergman, S.C., Corrigan, J., 1996. Compositional variation of natural apatites subjected to fission track analysis. International Workshop on Fission-Track Dating Abstracts, Gent, Belgium, August 26–30, p. 7.

Binder, G., Troll, G., 1989. Coupled anion substitution in natural carbon-bearing apatites. Contrib. Mineral. Petrol. 101, 394–401.

Burtner, R.L., Nigrini, A., Donelick, R.A., 1994. Thermochronology of lower Cretaceous source rocks in the Idaho–Wyoming thrust belt. Am. Assoc. Pet. Geol. Bull. 78, 1613–1636.

Carlson, W.D., 1990. Mechanisms and kinetics of apatite fission-track annealing. Am. Mineral. 75, 1120–1139.

Carlson, W.D., Donelick, R.A., Ketcham, R.A., 1999. Variability of apatite fission-track annealing kinetics: I. Experimental results. Am. Mineral. 84, 1213–1223.

Carpéna, J., 1998. Uranium-235 fission track annealing in minerals of the apatite group: an experimental study. In: Van den haute, P., De Corte, F. (Eds.), Advances in Fission-Track Geochronology. Kluwer Academic Publishers, Dordrecht, pp. 81–92.

Crowley, K.D., Cameron, M., McPherson, B.J., 1990. Annealing of etchable fission-track damage in F-, OH-, Cl- and Sr-apatite: 1. Systematics and preliminary interpretations. Nucl. Tracks Radiat. Meas. 17, 409–410.

Crowley, K.D., Cameron, M., Schaefer, R.L., 1991. Experimental studies of annealing of etched fission tracks in fluorapatite. Geochim. Cosmochim. Acta 55, 1449–1465.

Dahl, P.S., 1997. A crystal-chemical basis for Pb retention and fission-track annealing systematics in U-bearing minerals, with implications for geochronology. Earth Planet. Sci. Lett. 150, 277–290.

Donelick, R.A., 1993. Apatite etching characteristics versus chemical composition. Nucl. Tracks Radiat. Meas. 21, 604.

Elliott, J.C., 1994. Structure and chemistry of the apatites and other calcium orthophosphates. Studies in Inorganic Chemistry 18. Elsevier, Amsterdam. 389 pp.

Fleet, M.E., Pan, Y., 1995. Crystal chemistry of rare earth elements in fluorapatite and some calc-silicates. Eur. J. Mineral. 7, 591–605.

Fleet, M.E., Pan, Y., 1997. Site preference of rare earth elements in fluorapatite: binary (LREE+HREE)-substituted crystals. Am. Mineral. 82, 870–877.

Fortier, S.M., Giletti, B.J., 1989. An empirical model for predicting diffusion coefficients in silicate minerals. Science 245, 1481–1484.

Gallagher, K., Brown, R., Johnson, C., 1998. Fission track analysis and its applications to geological problems. Annu. Rev. Earth Planet. Sci. 26, 519–572.

Gleadow, A.J.W., Duddy, I.R., 1981. A natural long-term track annealing experiment for apatite. Nucl. Tracks 5, 169–174.

Green, P.F., Duddy, I.R., Gleadow, A.J.W., Tingate, P.R., Laslett, G.M., 1985. Fission-track annealing in apatite: track length measurements and the form of the Arrhenius plot. Nucl. Tracks 10, 323–328.

Green, P.F., Duddy, I.R., Gleadow, A.J.W., Tingate, P.R., Laslett, G.M., 1986. Thermal annealing of fission tracks in apatite: 1. A qualitative description. Chem. Geol., Isot. Geosci. Sect. 59, 237–253.

Green, P.F., Duddy, I.R., Laslett, G.M., Hegarty, K.A., Gleadow, A.J.W., Lovering, J.F., 1989. Thermal annealing of fission tracks in apatite: 4. Quantitative modelling techniques and extension to geological timescales. Chem. Geol., Isot. Geosci. Sect. 79, 155–182.

Hill, R.J., Howard, C.J., 1986. A computer program for Rietveld analysis of fixed wavelength X-ray and neutron powder diffraction patterns. Australian Atomic Energy Commission (ANSTO), Report No. M112. Lucas Heights Research Laboratories, New South Wales, Australia.

Hughes, J.M., Cameron, M., Crowley, K.D., 1989. Structural variations in natural F, OH, and Cl apatites. Am. Mineral. 74, 870–876.

Hughes, J.M., Cameron, M., Crowley, K.D., 1990. Crystal structures of natural ternary apatites: solid solution in the $Ca_5(PO_4)_3X$ (X=F, Cl, OH) system. Am. Mineral. 75, 295–304.

Hughes, J.M., Cameron, M., Mariano, A.N., 1991a. Rare-earth-element ordering and structural variations in natural rare-earth-bearing apatites. Am. Mineral. 76, 1165–1173.

Hughes, J.M., Cameron, M., Crowley, K.D., 1991b. Ordering of divalent cations in the apatite structure: crystal structure refinements of natural Mn- and Sr-bearing apatite. Am. Mineral. 76, 1857–1862.

Kowallis, B.J., Christiansen, E.H., Everett, B.H., Crowley, K.D., Naeser, C.W., Miller, D.S., Deino, A.L., 1993. Possible secondary apatite fission track age standard from altered volcanic ash beds in the middle Jurassic Carmel formation, south-western Utah. Nucl. Tracks Radiat. Meas. 21, 519–524.

Laslett, G.M., Green, P.F., Duddy, I.R., Gleadow, A.J.W., 1987. Thermal annealing of fission tracks in apatite: 2. A quantitative analysis. Chem. Geol., Isot. Geosci. Sect. 65, 1–13.

LeGeros, Z.R., 1965. Effect of carbonate on the lattice parameters of apatite. Nature 206, 403–404.

Liu, Y., Comodi, P., 1993. Some aspects of the crystal-chemistry of apatites. Mineral. Mag. 57, 709–719.

Mackie, P.E., Elliott, J.C., Young, R.A., 1972. Monoclinic structure of synthetic $Ca_5(PO_4)_3Cl$, chlorapatite. Acta Crystallogr. B28, 1840–1848.

O'Sullivan, P.B., Parrish, R.R., 1995. The importance of apatite composition and single-grain ages when interpreting fission track data from plutonic rocks: a case study from the Coast Ranges, British Columbia. Earth Planet. Sci. Lett. 132, 213–224.

Ravenhurst, C.E., Roden, M.K., Willet, S.D., Miller, D.S., 1993. Dependence of fission track annealing on apatite crystal chemistry. Nucl. Tracks Radiat. Meas. 21, 622.

Rønsbo, J.G., 1989. Coupled substitutions involving REEs and Na and Si in apatites in alkaline rocks from the Ilimaussaq intrusion, South Greenland, and the petrological implications. Am. Mineral. 74, 896–901.

Seifert, W., Kaempf, H., Wasternack, J., 2000. Compositional variation in apatite, phlogopite and other accessory minerals of the

ultramafic Delitzsch Complex, Germany; implication for cooling history of carbonatites. Lithos 53, 81–100.

Sha, L.K., Chappell, B.W., 1999. Apatite chemical composition, determined by electron microprobe and laser-ablation inductively coupled plasma mass spectrometry, as a probe into granite petrogenesis. Geochim. Cosmochim. Acta 63, 3861–3881.

Shannon, R.D., 1976. Revised effective ionic radii and systematic studies of interatomic distances in halides and chalcogenides. Acta Crystallogr. A32, 751–767.

Siddall, R., Hurford, A.J., 1998. Semi-quantitative determination of apatite anion composition for fission-track analysis using infrared microspectroscopy. Chem. Geol. 150, 181–190.

Sommerauer, J., Katz-Lehnert, K., 1985. A new partial substitution mechanism of $CO_3^{2-}/CO_3OH^{3-}$ and $SiO_4^{4-}$ for the $PO_4^{3-}$ group in hydroxyapatite from the Kaiserstuhl alkaline complex (SW-Germany). Contrib. Mineral. Petrol. 91, 360–368.

Steven, T.A., Mehnert, H.H., Obradovich, J.D., 1967. Age of volcanic activity in the San Juan Mountains, Colorado. U.S. Geol. Surv. Prof. Papers 575-D, D47–D55.

Stormer, J.C., Pierson, M.L., Tacker, R.C., 1993. Variation of F and Cl X-ray intensity due to anisotropic diffusion in apatite during electron microprobe analysis. Am. Mineral. 78, 641–648.

Sudarsanan, K., Young, R.A., 1969. Significant precision in crystal structural details; Holly Springs hydroxyapatite. Acta Crystallogr. B25, 1534–1543.

Sudarsanan, K., Mackie, P.E., Young, R.A., 1972. Comparison of synthetic and mineral fluorapatite, $Ca_5(PO_4)_3F$, in crystallographic detail. Mater. Res. Bull. 7, 1331–1338.

Thompson, P., Wood, I.G., 1983. X-ray Rietveld refinement using Debye–Scherrer geometry. J. Appl. Crystallogr. 16, 458–472.

Young, E.J., Munson, E.L., 1966. Fluor-chlor-oxy-apatite and sphene from Crystal Lodge pegmatite near Eagle, Colorado. Am. Mineral. 51, 1476–1493.

Young, E.J., Myers, A.T., Munson, E.L., Conklin, N.M., 1969. Mineralogy and geochemistry of fluorapatite from Cerro de Mercado, Durango, Mexico. U.S. Geol. Surv. Prof. Papers 650-D, D84–D93.